Two-Dimensional Navier–Stokes Turbulence in Bounded Domains

H. J. H. Clercx[1]
e-mail: h.j.h.clercx@tue.nl

G. J. F. van Heijst

J.M. Burgers Centre for Fluid Dynamics,
Department of Physics,
Eindhoven University of Technology,
P.O. Box 513,
5600 MB Eindhoven, The Netherlands

In this review we will discuss recent experimental and numerical results of quasi-two-dimensional decaying and forced Navier–Stokes turbulence in bounded domains. We will give a concise overview of developments in two-dimensional turbulence research, with emphasis on the progress made during the past 10 years. The scope of this review concerns the self-organization of two-dimensional Navier–Stokes turbulence, the quasi-stationary final states in domains with no-slip boundaries, the role of the lateral no-slip walls on two-dimensional turbulence, and their role on the possible destabilization of domain-sized vortices. The overview of the laboratory experiments on quasi-two-dimensional turbulence is restricted to include only those carried out in thin electromagnetically forced shallow fluid layers and in stratified fluids. The effects of the quasi-two-dimensional character of the turbulence in the laboratory experiments will be discussed briefly. As a supplement, the main results from numerical simulations of forced and decaying two-dimensional turbulence in rectangular and circular domains, thus explicitly taking into account the lateral sidewalls, will be summarized and compared with the experimental observations. [DOI: 10.1115/1.3077489]

1 Introduction

Our understanding of two-dimensional (2D) turbulence has been improved substantially during the past decades. Theoretical models have been proposed, dedicated laboratory experiments have been set up, and numerical investigations have been carried out to elucidate many aspects of 2D turbulence. These aspects include, to mention only a few, the inertial range scaling of the energy spectrum, the scaling exponents of velocity and vorticity structure functions, and the probability density functions (PDFs) of velocity and vorticity increments. These studies also raised new questions concerning decay scenarios of freely evolving 2D turbulence, condensation phenomena, the role of coherent structures in forced and freely evolving 2D turbulence, etc. Moreover, some of these phenomena are directly related to the boundedness of the flow domain. For example, the quasistationary final states of decaying 2D turbulence in bounded domains depend crucially on the geometry.

An additional complication to validate numerical findings or theoretical concepts for 2D turbulence is the difficulty to set up laboratory experiments to generate suitable 2D flows. In the 2D turbulence community, laboratory experiments in shallow fluid layers or in soap films are rather popular, but these experiments suffer from bottom friction (electromagnetically driven shallow flows) or thickness fluctuations (soap films). Suitably prepared decaying turbulence experiments in linearly stratified or two-layer fluids suffer from substantial vertical shear. As a consequence, these turbulent flows behave actually as quasi-2D; the implications of the presence of certain weak three-dimensional (3D) effects are not always very clear, and it requires advanced measurement techniques to quantify these phenomena. However, accurate laboratory experiments addressing these issues are rather scarce.

Another intriguing phenomenon concerns the rather surprising effects of the lateral boundedness of the flow, in particular when the domain boundaries consist of no-slip walls. In decaying 2D turbulence in square domains, the flow acquires spontaneously and rapidly angular momentum of either sign and subsequently decays slowly without changing the sign of the circulation of the large-scale central vortex that emerged during the decay process. This process is virtually absent in circular containers; it apparently depends on the domain geometry. Forced 2D turbulence simulations with certain specified forcing protocols revealed a similar phenomenon: a sequence of spontaneous spin-up of the flow, followed by a sudden breakdown of the central vortex due to severe vortex-wall interactions, and subsequent buildup of the large-scale vortex once again. This process goes on indefinitely, and the sign of the large-scale central vortex seems to be chosen randomly during each event of spin-up. One might wonder how 2D turbulence in such domains is affected by angular momentum production. Another question that arises concerns the production of small-scale vorticity at no-slip walls. The interaction of vortices with a no-slip wall leads to the formation of a thin boundary layer. In most cases such boundary layers detach and roll up to form small vortices containing high-amplitude vorticity. Recently, some evidence emerged that the small-scale vorticity produced at the boundaries might influence the scaling properties of 2D turbulence near the boundaries by introducing (weak) intermittency.

Bounded 2D turbulent flows, spontaneous spin-up phenomena, and quasi-two-dimensionality will be central topics in this review. We nevertheless start with a summary of a few highlights of 2D turbulence research from the past 4 decades in order to provide a framework to review 2D turbulence in domains with rigid no-slip walls. For a comprehensive overview of the developments until 1980, the review on hydrodynamic and plasma applications by Kraichnan and Montgomery [1] can be consulted. Danilov and Gurarie [2] gave an overview of quasi-2D and geostrophic turbulence and discussed observations and laboratory experiments with emphasis on geophysical applications. A recent review by Tabeling [3] provides a rather complete overview from a physicist's point of view of the developments up to the beginning of this century. This includes discussions of the equilibrium states of 2D turbulence, particle dispersion in 2D turbulence, and the role of coherent structures. For a more extensive review of some recent experiments, see Kellay and Goldburg [4] and references therein. We do not review many of the developments in the field of mathematical fluid dynamics and its application to 2D turbulence. Recent developments in this field are reported in a special issue of the Journal of Mathematical Physics (2007), and more relevant references can be found there [5].

2 Two-Dimensional Turbulence Without Boundaries

The starting point in the theoretical or numerical study of homogeneous 2D turbulence is the assumption that the 2D turbulent

[1]Also at Department of Applied Mathematics, University of Twente, P.O. Box 217, 7500 AE Enschede, The Netherlands.

Published online February 13, 2009. Transmitted by Assoc. Editor J. N. Reddy.

flow lives either in an unbounded domain or in a double-periodic square domain $\mathcal{D}$. Consider the 2D motion of a fluid on the domain $\mathcal{D}$ with boundary $\partial\mathcal{D}$. Cartesian coordinates in a frame of reference are denoted by x and y. Let the (horizontal) flow field be given by $\mathbf{u}=(u,v,0)$ with the vorticity $\boldsymbol{\omega}=\boldsymbol{\nabla}\times\mathbf{u}=(0,0,\omega)$, where $\omega=\partial v/\partial x-\partial u/\partial y$. The Navier–Stokes equations read

$$\frac{\partial \mathbf{u}}{\partial t}+\mathbf{u}\cdot\boldsymbol{\nabla}\mathbf{u}=-\frac{1}{\rho}\boldsymbol{\nabla}p+\sum_s \mathbf{D}_s+\mathbf{F} \tag{1}$$

$$\boldsymbol{\nabla}\cdot\mathbf{u}=0 \tag{2}$$

with p as the pressure and ρ as the fluid density. Here, $\mathbf{F}$ represents a possible external driving force. The dissipation term is denoted by

$$\mathbf{D}_s=(-1)^{s+1}\nu_s\boldsymbol{\nabla}^{2s}\mathbf{u} \quad \text{with} \quad s=\ldots,-2,-1,0,1,2,\ldots \tag{3}$$

Most cases discussed in this review concern Newtonian dissipation; thus $\mathbf{D}_1=\mathbf{D}=\nu\boldsymbol{\nabla}^2\mathbf{u}$, with ν as the kinematic viscosity. In some of the numerical studies mentioned below, a suitable combination of hyperviscous ($s\geq 2$, ultraviolet (UV) sink), hypoviscous ($s\leq -1$, infrared (IR) sink) dissipation or linear drag ($s=0$) is used, but all results for bounded flows with no-slip walls rely on Newtonian dissipation.

By taking the curl of Eq. (1), and assuming Newtonian dissipation, one obtains the vorticity equation

$$\frac{\partial \omega}{\partial t}+(\mathbf{u}\cdot\boldsymbol{\nabla})\omega=\nu\boldsymbol{\nabla}^2\omega+Q \tag{4}$$

with $\mathbf{Q}=\boldsymbol{\nabla}\times\mathbf{F}=(0,0,Q)$. The main difference between the scalar vorticity equation (4) and its 3D counterpart is the absence in the scalar vorticity equation of the term $(\boldsymbol{\omega}\cdot\boldsymbol{\nabla})\mathbf{u}$. This term represents the stretching and tilting of vortex tubes in 3D flows, leading to the formation of small intense vorticity filaments. As a consequence of the absence of vortex stretching and tilting, freely evolving 2D turbulence in unbounded domains cannot generate small-scale intense vortices. As we will see later on, the situation changes drastically with the presence of no-slip boundaries.

The main significant difference between 2D and classical 3D turbulence consists in the formation and persistence of large coherent structures (vortices) in 2D turbulence. The emergence of large-scale coherent structures was already predicted on theoretical grounds by Onsager [6] and Fjørtoft [7]. Any numerical or experimental investigation is inevitably carried out in a finite-sized domain. However, in any bounded situation, eventually the assumed classical Kolmogorov symmetries of homogeneity and isotropy are invalidated. As soon as the vortices have grown big enough to fill up the domain, then these symmetries no longer apply, and power-law spectra, derived on the assumption of an infinite region in which these symmetries prevail, become suspect. One should keep in mind that difficulties that have arisen in making the celebrated dual-cascade power-law predictions, see Sec. 2.1, to fit well with experimental or numerical data might be due to the eventual breakdown of these symmetries.

Before reviewing the main results obtained for 2D turbulence according to Eqs. (1)–(3), thus including dissipation, we briefly mention the statistical description of ideal homogeneous turbulence where dissipation is absent. This description is based on a Fourier representation of the dynamical variables; the finite number of Fourier coefficients forms a canonical ensemble. It was Lee [8] who realized that a finite Fourier representation of ideal 2D fluid dynamics [9] satisfies a Liouville theorem. The absolute equilibrium canonical (Gibbs) ensemble used to describe ideal 2D turbulence has played a role in identifying the tendencies for energy to accumulate in the smallest allowed wave number, which eventually dominates the energy spectrum [10]. In a broader context Shebalin [11] explored numerically the ergodic properties of ideal 2D turbulence (Euler turbulence) and ideal 2D magnetohydrodynamic (MHD) turbulence. It was found that 2D Euler turbulence appears ergodic, and evidence of a lack of ergodicity is shown for ideal 2D magnetohydrodynamic turbulence. In the latter case nonergodicity is due to the existence of disjoint components in the associated Fourier modal phase space. A phase point is confined to a restricted area of phase space and thus cannot get everywhere: the system exhibits broken ergodicity. The phase-space structure of finite Fourier representations of ideal, incompressible, homogeneous fluid and MHD turbulence (both 2D and 3D) was further investigated in more detail by Shebalin [12] later on. It was pointed out that nonergodicity can be attributed to the presence of helical invariants of the flow, which are present for 3D Euler and MHD flows (all examples showing nonergodicity) and absent for 2D Euler flows. Although dissipative effects are excluded in the analysis, the absolute equilibrium ensemble has proved to be a reliable predictor of inverse cascade behavior in 2D turbulence, and its utility has thus not been limited to 2D Euler flows.

2.1 Forced 2D Turbulence: The Inverse Energy and Direct Enstrophy Cascades. With the theoretical predictions by Onsager [6] and Fjørtoft [7] at hand, new attempts to formulate a phenomenological theory of 2D turbulence were put forward almost 40 years ago by Kraichnan [10,13], Leith [14], and Batchelor [15], known as the KLB theory. The statistical description of 2D turbulence in the KLB theory is based on the assumptions of homogeneity and isotropy in the limit of infinite domain size. In the inviscid limit, both the kinetic energy of the flow, $E=\frac{1}{2}\int_{\mathcal{D}}|\mathbf{u}|^2dA \geq 0$, with dA an infinitesimal area element, and the vorticity of fluid parcels are conserved. The latter actually implies an infinite number of conserved quantities, such as $\int_{\mathcal{D}}\omega^n dA$. Kraichnan [10] considered only two of them, the kinetic energy and the enstrophy $\Omega=\frac{1}{2}\int_{\mathcal{D}}\omega^2 dA\geq 0$, and proposed the existence of a dual cascade in forced unbounded 2D turbulence: the inverse energy cascade and the direct enstrophy cascade. Assuming a certain injection scale of kinetic energy, which in wave number space will be denoted by k_f, it is possible to make the following simplified picture of these cascades. With the assumption of the presence of a constant energy flux from the injection scale toward the largest scales accessible to the flow and the absence of enstrophy flux toward the smallest (and dissipative) scales, Kraichnan [10] predicted an inertial range scaling as $E(k)=C_1\epsilon^{2/3}k^{-5/3}$, with ϵ as the rate of cascade of kinetic energy per unit mass and C_1 as the Kolmogorov–Kraichnan constant. The other case concerns the situation with the presence of a constant enstrophy flux from the injection scale toward the dissipative scales and the absence of energy flux toward the largest scales, and an inertial range according to $E(k)=C_2\eta^{2/3}k^{-3}$ has been predicted (with a logarithmic correction, see Kraichnan [13]). Here, η is the rate of cascade of mean-square vorticity and C_2 is the Kraichnan–Batchelor constant.

The first direct numerical simulations (DNS) of forced 2D turbulence with periodic boundary conditions were carried out by Lilly [16] in order to confirm the existence of the dual cascade. These numerical studies were restricted to a resolution of 64^2 grid points, definitely a too low resolution. Nevertheless, these results indicate the presence of a $k^{-5/3}$ and a k^{-3} inertial range in line with the Kraichnan prediction. For obtaining such results, a forcing [17] should be applied, which is spectrally localized to a wave number interval $(k_f,k_f+\Delta k)$, with $\Delta k\ll k_f$. Moreover, the domain size, the forcing scale, and the dissipative scales should be sufficiently separated. Obviously, numerical experiments aimed at simultaneously generating both 1–2 decade inverse energy and direct enstrophy cascades require therefore extremely high resolutions. Only very recently Boffetta [18] reported on a very high resolution (up to $16,384^2$ grid points, or using 8192^2 Fourier modes) simulation of stationary 2D turbulence. He used a forcing that is narrow banded in space and short correlated in time with a forcing scale of $l_f=L/100$, with L as the box size. Thus approxi-

mately 2 decades are available for both the inverse energy cascade and the direct enstrophy cascade. Linear damping has been used to remove energy at large scales by friction, and classical Newtonian viscosity is used for dissipation at small scales. This DNS of the 2D Navier–Stokes equations indeed reproduces, for the first time, the dual-cascade scenario predicted by Kraichnan [10].

Many attempts have been pursued to perform simulations generating only one of the two inertial ranges. The first observations of the inverse energy cascade, besides the study mentioned earlier [16], are those by Fyfe et al. [19] and Hossain et al. [20] on forced 2D magnetohydrodynamics, by Frisch and Sulem [21], and by Herring and McWilliams [22]. The simulations by Frisch and Sulem [21] were based on 256^2 grid points with random forcing in the wave number range $13 < k_f < 17$, and a clear inverse cascade range with $k^{-5/3}$ scaling was observed. Measurement of the Kolmogorov–Kraichnan constant gave the value $C_1 \approx 9 \pm 2$, in a similar range as predicted with the test field model [13], viz., $6 < C_1 < 7$. Siggia and Aref [23] obtained the $k^{-5/3}$ scaling for the inverse energy cascade with point-vortex simulations using 128^2 point vortices. They found, however, a value for the Kolmogorov–Kraichnan constant somewhat at odds with other investigations, $C_1 \approx 14$. One of the most accurate studies on the scaling of the inertial range for the inverse cascade is the work by Smith and Yakhot [24]. A pseudospectral simulation with 2048^2 Fourier modes, with $\mathbf{D}_8$ dissipation (3), and with forcing in the interval $500 \leq k_f \leq 525$ yielded a scaling behavior over 2 decades, $E(k) \propto k^{-n}$, with $n = -\frac{5}{3} \pm 0.05$. Moreover, they found that $C_1 \approx 7.0$. Another remarkable observation by Smith and Yakhot [24], already predicted by Kraichnan [10], is the formation of a large-scale structure akin a Bose–Einstein condensate (in a similar run with 512^2 Fourier modes and $100 \leq k_f \leq 105$). Here, all the energy that cascades from the injection scale toward the large scales ($k \approx 1$) is collected in this structure. The emerging large-scale structure has a dipolelike character, and previous indications of this phenomenon was already reported in the study by Hossain et al. [20]. Recently, the dynamics of energy condensation was studied in more detail by Chertkov et al. [25]. They showed a self-similar growth of the domain-sized dipolar vortex and showed that it indeed contains most of the injected energy. The numerical study by Borue [26], using hyper- and hypoviscous dissipation operators ($\mathbf{D}_8$ and $\mathbf{D}_{-8}$, respectively), revealed a different picture. Borue [26] carried out one simulation with a 512^2 resolution (and Gaussian white-in-time forcing with $100 \leq k_f \leq 102$) and two simulations with a 1024^2 resolution (the latter two with $250 \leq k_f \leq 252$ and $350 \leq k_f \leq 352$, respectively). The measured inverse energy spectrum shows initially a $k^{-5/3}$ range but steepens later on to yield a k^{-3} scaling. This was accompanied by the emergence of a large number of strong vortices. Danilov and Gurarie [2,27] attributed the anomalous scaling behavior observed by Borue [26] to the use of infrared dissipation. Applying linear drag yields a nearly perfect $-5/3$ slope (but a nonuniform energy flux). More recently, Boffetta et al. [28] performed pseudospectral simulations with 2048^2 Fourier modes, employing hyperviscous dissipation ($\mathbf{D}_8$) and linear damping ($\mathbf{D}_0$) to avoid the buildup of the condensate state, reported a clear inverse cascade, and found $C_1 = 6.0 \pm 0.4$. In a similar spirit, Chen et al. [29] obtained an inverse cascade over nearly 2 decades (using 2048^2 Fourier modes, $k_f \approx 500$, and dissipation operators $\mathbf{D}_{-2}$ and $\mathbf{D}_8$ as IR and UV sink, respectively) (see Fig. 1).

The physical picture of the processes dominating the enstrophy cascade is the elongation of weak vorticity patches in random large-scale strain. Due to mass conservation, vorticity patches conserve area. As a result, elongation in one direction must imply compression in the other direction, and vorticity gradients will steepen. For (nearly) inviscid fluids, the vorticity of fluid parcels is (approximately) conserved, and a process of stretching and folding of fluid elements by the random large-scale strain field continues and yields the formation of thin vorticity filaments. This

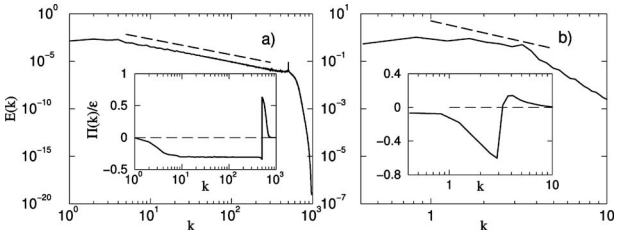

Fig. 1 Energy spectrum $E(k)$ versus k at steady state obtained by (*a*) DNS and (*b*) shallow fluid-layer experiments. The dashed line has a slope of −5/3. Insets: spectral energy flux $\Pi(k)/\epsilon$ from (*a*) DNS and (*b*) experiment, with ϵ as the net energy dissipation at all scales. Courtesy of Chen et al. [29].

phenomenon is the physical-space interpretation of the nonlocality of the enstrophy cascade: small scales (weak vortices) are directly affected by large scales (strong strain). This nonlocality of the enstrophy cascade was already recognized by Kraichnan [13]. The filaments become so thin that finally diffusion of vorticity will start to dominate the transport processes; i.e., the length scale associated with the filament thickness is comparable with the viscous length scale $l_d = (\nu^3/\eta)^{1/6}$. It is noteworthy to mention here an alternative scaling for the enstrophy cascade compared with the classical Kraichnan–Batchelor picture. Saffman [30] investigated the implications of the presence of many filamentary vorticity structures on the energy spectrum and proposed a k^{-4} spectrum. Moffatt [31] emphasized the importance of spiral-like structures and proposed a $k^{-11/3}$ spectrum.

The enstrophy cascade is usually studied by employing low wave number forcing so that the full resolution can be used for the enstrophy cascade. Confirmation of the classical behavior of the direct enstrophy cascade, i.e., numerical observation of the k^{-3} scaling of the spectrum, has been reported by several investigators, provided that one is able to destroy long-lived coherent structures. These structures might emerge as a result of the forcing protocol. Herring and McWilliams [22] showed that the enstrophy spectrum steepens in the presence of persistent coherent vortices due to partial disruption of the direct enstrophy cascade. However, adaptation of the forcing in such a way that long-lived vortices are virtually absent yields the classical enstrophy cascade. Similar observations were reported in several studies [32–34]. On the other hand, Borue [35] reported a k^{-3} scaling for the direct enstrophy cascade with a series of stationary forced 2D turbulence simulations both with normal viscosity (resolutions up to 4096^2 Fourier modes) and with hyperviscosity (by using $\mathbf{D}_8$; resolutions up to 2048^2 Fourier modes). The computations with hyperviscosity provided evidence for a constant enstrophy flux over approximately 2 decades of wave numbers. An estimate for the Kraichnan–Batchelor constant obtained from this study is $C_2 \approx 1.5-1.7$. The work by Borue [35], showing evidence of a direct enstrophy cascade over almost 2 decades, suggests that the logarithmic correction to the k^{-3} scaling as predicted by Kraichnan [13] might be within range. Nevertheless, it seems that the logarithmic factor is difficult to detect in numerical simulations [36–40], which might also be related to the choice of dissipation operators. For example, Gotoh [36] used Newtonian dissipation and $\mathbf{D}_{-1}$ as IR sink; Lindborg and Älvelius [37] used $\mathbf{D}_{-2}$ and $\mathbf{D}_2$ hypo- and hyperviscous dissipation operators, respectively. Both used resolutions of 4096^2 modes but found it difficult to observe the logarithmic correction. The recent results by Chen et al. [40] seem consistent with the proposed logarithmic correction (they used $\mathbf{D}_{-2}$ as IR and $\mathbf{D}_8$ as UV sink, and could therefore use lower resolutions, i.e., 2048^2 Fourier modes) (see Fig. 2). It should be mentioned here that the runs by Borue [35] with normal viscosity did not show a very clear k^{-3} scaling, but the trends toward it and toward a constant enstrophy flux could be observed.

These numerical studies confirm several aspects of the KLB

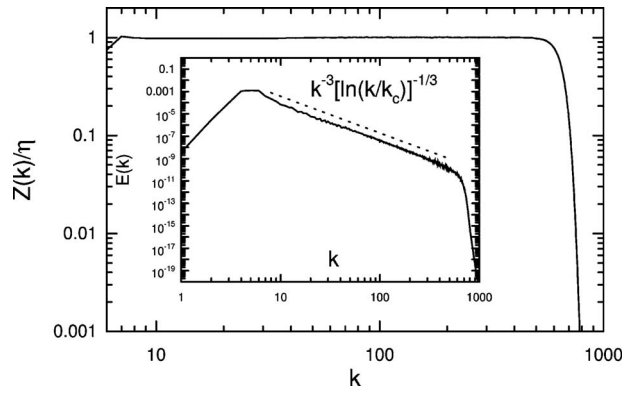

Fig. 2 Enstrophy flux $Z(k)$ normalized by enstrophy dissipation η versus k. The inset is the energy spectrum. Courtesy of Chen et al. [40].

theory, but the assumptions of this theory, the resulting scaling laws, and the universality of the inverse energy and direct enstrophy spectra have been questioned in recent years. It is found essential that intermittency is absent and the flow is largely free of coherent vortices. One of the other issues concerns the debate on whether the KLB theory, derived for the infinite 2D domain, holds on a bounded doubly periodic domain. Tran and Shepherd [41] and Tran and Bowman [42] addressed the validity of the dual-cascade picture for forced 2D turbulence in bounded domains (with periodic boundaries) and concluded that the KLB dual-cascade picture is a phenomenon strictly related to the unboundedness of the system. It was shown by Tran and Shepherd [41] that a steady-state enstrophy cascade (with k^{-3} scaling) is unrealizable in a bounded domain for a constant monoscale forcing and Newtonian dissipation. They also observed that the KLB scaling applies in the enstrophy-cascading range, provided that together with Newtonian dissipation also hypoviscous dissipation, $\mathbf{D}_s$ with $s<0$, is invoked. Gotoh [36] and Borue [35] used hypoviscous dissipation of this form and found evidence of the k^{-3} scaling. Quite remarkably, k^{-3} scaling is also found using hypo- and hyperviscous dissipation operators [37,40] and using linear drag and hyperviscous dissipation [38,39]. In order to shed some more light on these issues, Alexakis and Doering [43] derived some rigorous upper bounds on the bulk energy dissipation rate ϵ and the enstrophy dissipation rate η for 2D statistically stationary flows in bounded domains sustained by various driving forces. They applied more general types of forcing than monoscale forcing [41] and considered also forcing that varies smoothly in time (in contrast to temporally white-noise forcing [44]). For a broad class of driving forces, Alexakis and Doering [43] found the following upper bounds for the dimensionless energy and enstrophy dissipation rates: $\tilde{\epsilon} \lesssim \mathrm{Re}^{-1/2}$ and $\tilde{\eta} \lesssim \mathrm{Re}^{0}$. In the inviscid limit ϵ vanishes as fast as $\mathrm{Re}^{-1/2}$, and $\epsilon \to 0$ and $\eta = \mathcal{O}(1)$ are consistent with the KLB theory. For narrow-band monochromatic forcing, Alexakis and Doering [43] reported $\tilde{\epsilon} \lesssim \mathrm{Re}^{-1}$ and $\tilde{\eta} \lesssim \mathrm{Re}^{-1}$ consistent with results by Tran and Shepherd [41] and by Eyink [44]. In this case, both ϵ and η vanish in the inviscid limit, suggesting essentially laminar behavior of the flow. Tran and Shepherd [41] interpreted this as absence of a direct enstrophy cascade for statistically stationary flows in bounded domains. However, their results rely on special forcing conditions that are not guaranteed for general forcing procedures.

In recent years renewed emphasis has been given to the physical mechanisms of the 2D enstrophy and inverse energy cascades by Chen et al. [29,40] and those of scale-to-scale transfers of passive-tracer variance in 2D turbulence [45,46]. The latter studies are based on an investigation of the dynamics of tracer increments (structure functions). The first of the two contributions by Chen et al. [40] focused on the spatial distribution of the enstrophy transfer. They considered the local flux that quantifies the enstrophy transfer into small scales at fixed points in real space and distinguished large- and small-scale modes with a filtering procedure (analogous to modeling in large-eddy simuations (LES)). The filter is applied on the 2D Euler equation $\partial_t \omega + (\mathbf{u}\cdot\nabla)\omega = 0$. They introduced the large-scale vorticity $\bar{\omega}_l = \mathcal{G}_l * \omega$ and the large-scale velocity $\bar{\mathbf{u}}_l = \mathcal{G}_l * \mathbf{u}$, where $\mathcal{G}_l$ is a Gaussian filter with filter width l. The 2D Euler equation after low-pass filtering becomes

$$\frac{\partial \bar{\omega}_l(\mathbf{r},t)}{\partial t} + \nabla \cdot [\bar{\mathbf{u}}_l(\mathbf{r},t)\bar{\omega}_l(\mathbf{r},t) + \boldsymbol{\sigma}_l(\mathbf{r},t)] = 0 \tag{5}$$

where $\boldsymbol{\sigma}_l = \overline{(\mathbf{u}\omega)}_l - \bar{\mathbf{u}}_l\bar{\omega}_l$. This quantity represents the spatial transport of vorticity as a result of the small-scale turbulence. Multiplying Eq. (5) by $\bar{\omega}_l(\mathbf{r},t)$, introducing the local enstrophy density $\Omega_l(\mathbf{r},t) = \frac{1}{2}\bar{\omega}_l^2(\mathbf{r},t)$ based on the filter width l, and some rewriting yields the following balance equation for the local enstrophy density:

$$\frac{\partial \Omega_l(\mathbf{r},t)}{\partial t} + \nabla \cdot \mathbf{K}_l(\mathbf{r},t) = -Z_l(\mathbf{r},t) \tag{6}$$

Here, the current $\mathbf{K}_l(\mathbf{r},t)$ represents the spatial transport of large-scale enstrophy and $Z_l(\mathbf{r},t)$ represents the enstrophy flux from large scales ($\geq l$) into small scales ($\leq l$). Expressions for the current $\mathbf{K}_l$ and the enstrophy flux Z_l are

$$\mathbf{K}_l(\mathbf{r},t) = \Omega_l(\mathbf{r},t)\bar{\mathbf{u}}_l(\mathbf{r},t) + \bar{\omega}_l(\mathbf{r},t)\boldsymbol{\sigma}_l(\mathbf{r},t) \tag{7}$$

and

$$Z_l(\mathbf{r},t) = -\nabla\bar{\omega}_l(\mathbf{r},t)\cdot\boldsymbol{\sigma}_l(\mathbf{r},t) \tag{8}$$

The presence of a forward enstrophy cascade requires that $Z_l(\mathbf{r},t)$ has a net positive value, which indicates that the turbulent vorticity transport vector $\boldsymbol{\sigma}_l$ tends to be down-gradient, i.e., antiparallel to the large-scale vorticity gradient $\nabla\bar{\omega}_l$. Keeping in mind that vorticity gradients tend to be perpendicular to streamlines, the antiparallel alignment would suggest that turbulent vorticity transport is perpendicular to the large-scale velocity.

Chen et al. [40] studied the statistical anticorrelation of $\boldsymbol{\sigma}_l$ and $\nabla\bar{\omega}_l$ by analyzing the PDF of the enstrophy flux in the steady-state cascade and of the angle of alignment θ between the vectors $\boldsymbol{\sigma}_l$ and $\nabla\bar{\omega}_l$ (θ is defined by $Z_l = |\boldsymbol{\sigma}_l||\nabla\bar{\omega}_l|\cos(\pi-\theta)$). For this purpose they performed numerical simulations with forcing in the wave number band $4 \leq k_f \leq 7$. The resulting direct enstrophy cascade (with constant enstrophy flux η) extended up to almost 2 decades.

For several filter widths, the normalized PDF of $Z_l - \langle Z_l\rangle$ has been computed, and it appears to be only slightly asymmetric (the skewness is found to be rather small) and its shape resembles the experimentally measured PDFs in soap films by Rivera et al. [47]. The PDF of the angle of alignment θ revealed a greater probability for $\theta > \pi/2$, indicating a positive enstrophy flux. The most probable value for θ is about 103 deg, far from 180 deg, but still sufficient to support a positive enstrophy flux to small scales. This analysis clearly indicates that turbulent vorticity transport tends to be on average virtually parallel to the large-scale velocity. Further analysis revealed the correctness of the classical picture that the forward enstrophy cascade predominantly occurs in strain regions [15,48], i.e., stretching of small-scale vorticity gradients as a result of strain induced by the larger-scale vortices (nonlocal transfer).

In a similar spirit, Chen et al. [29] and Eyink [49,50] analyzed the physical mechanism of the 2D inverse energy cascade. In the 1970s Kraichnan [13,51] came up with a heuristic idea to account for the 2D inverse energy cascade by postulating a constitutive law for the turbulent stress: $\boldsymbol{\tau} = -2\nu_T\mathbf{S}$, with $\boldsymbol{\tau}$ as the turbulent stress and $\mathbf{S}$ as the strain, and introducing a negative eddy viscosity $\nu_T < 0$. The negative eddy viscosity can be understood intu-

itively as a consequence of the thinning of small-scale vortices by strain at much larger scales. Eyink [49,50] and Chen et al. [29] showed, however, that the inverse cascade mainly results from turbulent stress proportional to small-scale strain rotated by 45 deg (or skew strain) with respect to the large-scale strain.

Chen et al. [29] focused on the energy flux across a length scale l in the inertial range. A quantitative analysis is once again based on distinguishing the large- and small-scale modes with a filtering procedure (with filter width l) as outlined above. Low-pass filtering of Eq. (1) gives

$$\frac{\partial \overline{\mathbf{u}}_l(\mathbf{r},t)}{\partial t} + \boldsymbol{\nabla}\cdot[\overline{\mathbf{u}}_l(\mathbf{r},t)\overline{\mathbf{u}}_l(\mathbf{r},t) + \boldsymbol{\Sigma}_l(\mathbf{r},t)] = -\frac{1}{\rho}\boldsymbol{\nabla}\,\overline{p}_l(\mathbf{r},t) + \mathbf{D}_{-2} \tag{9}$$

where $\boldsymbol{\Sigma}_l = \overline{(\mathbf{uu})}_l - \overline{\mathbf{u}}_l\overline{\mathbf{u}}_l$ is the stress tensor induced by eddies at scales smaller than l. It should be noted here that low-pass filtering removes the hyperviscous dissipation operator (assuming it is only active at scales much smaller than l) and that the action of the hypoviscous dissipation is virtually unaffected by filtering because it acts only on box-size coherent structures. These have a much larger size than the filter width. The local kinetic energy density is $E_l(\mathbf{r},t) = \frac{1}{2}|\overline{\mathbf{u}}_l(\mathbf{r},t)|^2$, and the energy equation after low-pass filtering becomes

$$\frac{\partial E_l(\mathbf{r},t)}{\partial t} + \boldsymbol{\nabla}\cdot\mathbf{J}_l(\mathbf{r},t) = -\Pi_l(\mathbf{r},t) + \overline{\mathbf{u}}_l(\mathbf{r},t)\cdot\mathbf{D}_{-2} \tag{10}$$

Here, the current $\mathbf{J}_l(\mathbf{r},t)$ represents the spatial energy transport and $\Pi_l(\mathbf{r},t)$ represents the energy flux to scales $\lesssim l$ at each point in space. Expressions for the current $\mathbf{J}_l$ and energy flux Π_l are [49]

$$\mathbf{J}_l(\mathbf{r},t) = \left[E_l(\mathbf{r},t) + \frac{\overline{p}_l(\mathbf{r},t)}{\rho}\right]\overline{\mathbf{u}}_l(\mathbf{r},t) + \overline{\mathbf{u}}_l(\mathbf{r},t)\cdot\boldsymbol{\Sigma}_l(\mathbf{r},t) \tag{11}$$

and

$$\Pi_l(\mathbf{r},t) = -\tfrac{1}{2}(\boldsymbol{\nabla}\overline{\mathbf{u}}_l(\mathbf{r},t) + [\boldsymbol{\nabla}\overline{\mathbf{u}}_l(\mathbf{r},t)]^T):\boldsymbol{\Sigma}_l(\mathbf{r},t) \tag{12}$$

Evidently, Eq. (12) is the scalar product of the strain from scales $\gtrsim l$ and the stress from scales $\lesssim l$ and represents the rate of work done by the large-scale velocity gradient against the small-scale stress. This rate of work is positive when the small-scale stress resists the large-scale strain (forward cascade), and it is negative when the large-scale strain is reinforced by the small-scale stress (inverse cascade). They performed numerical simulations (details already mentioned earlier) and computed the spatial distribution of $\Pi_l(\mathbf{r},t)$. It is revealed that certain regions are characterized by a forward cascade, and other regions by an inverse cascade. On average the cascade is backward [29].

A deeper insight into the physical mechanisms has been gained by applying a multiscale gradient (MSG) expansion of the turbulent stress tensor $\boldsymbol{\Sigma}_l$, a new analytical approach proposed by Eyink [49,50]. He showed, by expanding the stress $\boldsymbol{\Sigma}_l$ into a convergent series of quadratic products of gradients of the velocity at scale $l_n = 2^{-n}l < l$ and by considering for the moment only contributions that are first order in gradients, that the contribution to the stress from length scale l_n can be approximated by

$$\boldsymbol{\Sigma}^{(n)}_{\mathrm{MSG}} = C^{(n)} l_n^2 \boldsymbol{\omega}^{(n)}\widetilde{\mathbf{S}}^{(n)} \tag{13}$$

Here $C^{(n)}$ is a constant and $\boldsymbol{\omega}^{(n)}$ is the vorticity at scale l_n. The tensor $\widetilde{\mathbf{S}}^{(n)}$ is the strain tensor $\mathbf{S}^{(n)}$ at scale l_n rotated counterclockwise by 45 deg and is referred to as the skew strain. A physical interpretation of the inverse cascade supporting relation (13) is the following. Consider a small-scale vortex in a large-scale strain field. This vortex will be elongated along the stretching direction of the strain field and thinned in the compressing direction (see Fig. 3). Conservation of mass and circulation requires that the velocity around the elongated vortex is reduced with respect to the nonelongated vortex; thus the kinetic energy of the vortex is also reduced. The vortex is rectified to a narrow shear layer with its major axis almost parallel to the stretching axis and produces a net positive stress along this axis. The energy lost by the small-scale vortex is thus used to reinforce the large-scale strain, and in this way the small-scale energy is transferred to the larger scales. The small-scale strain basis associated with the elongated vortex is rotated relative to the large-scale strain basis by $\pi/4$ rad in clockwise or anticlockwise direction, depending on the sign of the small-scale vorticity. Eyink [49,50] showed that the stress is then proportional to $\omega^{(n)}\widetilde{\mathbf{S}}^{(n)}$. Supporting numerical and experimental evidence is provided in the study by Chen et al. [29].

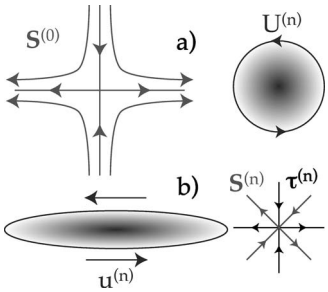

Fig. 3 Vortex-thinning mechanism: (*a*) small-scale circular vortex in a large-scale strain field $S^{(0)}$; (*b*) small-scale vortex drawn out into a narrow shear layer with weakened velocity $u^{(n)} < U^{(n)}$. The axes of the small-scale stress tensor $\tau^{(n)}$ are aligned with those of the large-scale strain $S^{(0)}$, whereas the small-scale strain $S^{(n)}$ axes are rotated at $\pm\pi/4$ rad with respect to $S^{(0)}$. Courtesy of Chen et al. [40].

Boffetta [18] applied the methods introduced by Chen et al. [29,40] and Eyink [50] to study the distribution of spatial fluxes obtained with his dual-cascade computation mentioned earlier. Also this computation shows nearly symmetric PDFs of the local energy and enstrophy fluxes $\Pi_l(\mathbf{r},t)$ (see Eq. (12)) and $Z_l(\mathbf{r},t)$ (see Eq. (8)), respectively, as previously observed by Chen et al. [29,40].

2.2 Decaying 2D Turbulence and Vortex Statistics. In 1971 Lilly [52] also focused attention on freely developing and decaying 2D turbulence in order to confirm the predicted scaling of the inertial range according to the KLB theory and to investigate whether the time-dependent behavior of the quadratic moments E and Ω and the palinstrophy $P = \frac{1}{2}\int_{\mathcal{D}}|\boldsymbol{\nabla}\omega|^2 dA \geq 0$, as predicted by Batchelor [15], could be recovered. The dissipation of kinetic energy and enstrophy in unbounded or periodic domains with finite viscosity ν is governed by the relations

$$\frac{dE(t)}{dt} = -2\nu\Omega(t) \quad \text{and} \quad \frac{d\Omega(t)}{dt} = -2\nu P(t) \tag{14}$$

From these two relations, it can directly be concluded that for decaying flows with finite viscosity both $E(t)$ and $\Omega(t)$ always decrease in the course of time. In particular, the enstrophy is bounded by its initial value, i.e., $\Omega(t) \leq \Omega(t=0)$ [53] implying that $dE/dt \to 0$ for $\nu \to 0$.

The investigation by Lilly [52], based on 64^2 grid points in the computational domain, supported the k^{-3} scaling for the direct enstrophy cascade albeit for the late decay stage. (Note that the Kraichnan–Batchelor theory also predicts a k^{-3} energy spectrum for decaying 2D turbulence.) Moreover, some support is provided for the following decay rates for large t: $E(t) \propto t^{-1}$, $\Omega(t) \propto t^{-2}$, and $P(t) \propto t^{-3}$. However, high-resolution simulations performed since the 1980s indicated that the agreement with Batchelor's prediction is due to the relatively low resolution, i.e., small Reynolds number, in these simulations.

The emergence of persistent weakly dissipative coherent vorti-

ces and the existence of a quasistationary "equilibrium" state were first reported in the late 1970s [54–56]. Convincing evidence of the emergence of long-lived coherent vortices, which persist for many (typical) eddy turnover times, from a zero-mean Gaussian random initial field with random phases in a decaying 2D turbulence simulation was reported by McWilliams [57]. The resolution of this kind of simulation is 256^2 spatial grid points and used hyperviscous dissipation, $\mathbf{D}_2$ (see Eq. (3)). In this latter study the initial kinetic energy spectrum is broadband and peaked around the wave number $k_0=6$, and the slope of the energy spectrum had a k^{-3} range for $k \gtrsim 10$. The spectrum steepened toward k^{-5}, and the enstrophy transfer dropped to zero. The energy spectra obtained in subsequent DNS studies [58] also showed that the direct enstrophy cascade is often only established as a transient state and steeper than predicted by Kraichnan [10] and Batchelor [15]. This was also attributed to the appearance of coherent vortices. In particular, Santangelo et al. [58] reported a systematic study, based on high-resolution simulations (1024^2 Fourier modes) and very long-time integrations, of two sets of initial conditions. The first with a steep initial energy spectrum, with $E(k) \sim k \exp(-k^2/k_0^2)$ (with random phases and $k_0 \sim 2-8$), and biharmonic hyperviscous diffusion was used. This is similar to the initialization used by Kida [59] and Brachet et al. [60,61] (although they used Newtonian dissipation). The second set has an initial energy spectrum close to the one of the Kraichnan–Batchelor theory ($E(k) \propto k^{-3}$ with random phases and using hyperviscous dissipation with $\mathbf{D}_2$). Such initial conditions were previously used by McWilliams [57] and by Benzi et al. [62,63]. Santangelo et al. [58] concluded that the formation of coherent vortices destroys the scale invariance and produces steep spectra, and they established that the k^{-3} enstrophy inertial range is obtained only as a transient state during the decay. Moreover, they observed that the long-term behavior strongly depends on the initial conditions.

Further analysis by McWilliams [64] revealed that the vortices can slow down the cascade processes. This was demonstrated by comparing the evolution of an initial vorticity field (same resolution and similar algorithm as used previously [57], but with a narrow-banded initial kinetic energy spectrum that is peaked around $k_0=15$) containing well-developed vortices with the decay of initial fields that have initially the same wave number spectra but lack vortices (by using phase scrambling). The simulations without vortices in the initial condition show substantially larger cascade rates. This can be understood by realizing that the vortices contain most of the enstrophy and that the stronger vortices usually do not destroy each other; thus stretching and filamentation effects will be relatively unimportant and cascade processes will be suppressed.

With the assumption of a finite enstrophy dissipation in the inviscid limit, Batchelor [15] used scaling arguments to predict the k^{-3} power-law behavior of the energy spectrum. Tran and Dritschel [65] recently revisited this issue and derived bounds on the enstrophy dissipation η for freely decaying 2D turbulence. These bounds are expressed in initial ideal invariants of the flow. They find in the limit $\mathrm{Re} \to \infty$ that $\eta \lesssim (\ln \mathrm{Re})^{-1/2}$, an extremely weak dependence on Re. The physical explanation is as follows. Decreasing viscosity results in enhanced production of palinstrophy and its dissipation. However, it seems that the net growth of the palinstrophy is less rapid than the decrease in viscosity; thus with $\eta=-2\nu P$ it follows that the enstrophy dissipation should vanish. It is nevertheless fair to conclude that Batchelor's argument of nonvanishing enstrophy dissipation is not so sensitive for this weak Re-dependence.

The emergence and the temporal evolution of a hierarchy of coherent vortices in decaying 2D turbulence have been subject to many analytical, numerical, and even experimental studies [66–72]. One of the most remarkable theoretical results of the past decade is the scaling theory, as proposed by Carnevale et al. [67,68]. In this theory it is supposed that the average number density of vortices decreases algebraically, $\rho(t) \propto t^{-\zeta}$, with ζ so far undetermined. Numerical simulations with a simple, punctuated-Hamiltonian, dynamical model for the evolution of a system of coherent vortices [67] and also numerical simulations of the Navier–Stokes equations, although hyperviscosity has been used, yielded the estimate [68,69,73] $\zeta \sim 0.72-0.75$.

This numerically measured value of the decay exponent suggests that the straightforward scaling theory by Batchelor [15] is incorrect. His theory is based on the assumption that for nearly inviscid 2D turbulent flows the energy might still be considered as conserved, but not the enstrophy, because viscosity is preferentially dissipative on the smallest scales of the flow. Dimensional analysis then results in $\rho(t) \propto t^{-2}$, which shows a large discrepancy with the approach of Carnevale et al. [67,68]. Besides energy conservation Carnevale et al. [67,68] also assumed that the extremum of vorticity, ω_{ext}, is conserved. Dimensional analysis then yields for the average number density $\rho(t) \propto L^{-2}(t/T)^{-\zeta}$, the average enstrophy $\Omega(t) \propto T^{-2}(t/T)^{-\zeta/2}$, the average vortex radius $a(t) \propto L(t/T)^{\zeta/4}$, and the average mean vortex separation $r(t) \propto L(t/T)^{\zeta/2}$. The characteristic length scale L and time scale T are defined by $L=\omega_{\mathrm{ext}}^{-1}\sqrt{E}$ and $T=\omega_{\mathrm{ext}}^{-1}$, respectively. As mentioned before, the power-law exponent is a free parameter, which has to be predicted on the basis of numerical simulations. Another remarkable consequence of this scaling theory is the rather small decay exponent for the enstrophy, $\Omega(t) \propto t^{-0.36}$ ($\zeta \approx 0.72$), compared with $\Omega(t) \propto t^{-2}$ derived by Batchelor [15].

In a recent work, Bracco et al. [72] revisited freely decaying 2D turbulence at very high resolution (4096^2 grid points and using $\mathbf{D}_2$). Their initial condition is given by a zero-mean Gaussian vorticity field with random Fourier phases. The kinetic energy spectrum was narrow banded and peaked at wave number $k_0=30$ and evolved into a spectrum with a slope steeper than k^{-3} due to the presence of many vortices. Their main findings confirm earlier results on vortex statistics [68,69,73], including conservation of vorticity inside vortex cores and the power-law behavior for the vortex number density. This study basically supports the scaling theory put forward by Carnevale et al. [67,68] although some discrepancies have been found. Bracco et al. [72] reported sets of power-law exponents obtained by two slightly different ensembles of vortices. Considering all vortices yielded $\zeta=0.76\pm0.03$, but the scaling exponents for the average vortex radius and the average vortex circulation, $\Gamma(t) \approx \omega_{\mathrm{ext}}(t)a^2(t) \propto t^{\zeta/2}$, did not agree very well. They found $a^4(t) \propto t^{\zeta_1}$, with $\zeta_1=0.94\pm0.10$, and $\Gamma^2(t) \propto t^{\zeta_2}$, with $\zeta_2=1.00\pm0.09$. The scaling theory of Carnevale et al. [67,68] dictates that $\zeta_1=\zeta_2=\zeta$. This discrepancy might partly be due to lack of conservation of $\omega_{\mathrm{ext}}(t)$, but it does not account fully for it. Alternative ensemble averaging, using only vortices with ω_{ext} exceeding a certain threshold value proved to yield better results, but some disagreements remain. Remarkably, ω_{ext} is found to be conserved, and the adapted decay exponent (based on the power law for the average vortex number) is now $\zeta=0.67\pm0.02$. Analyzing the average vortex radius and circulation yields $\zeta_1=0.68\pm0.04 \approx \zeta$ and $\zeta_2=0.84\pm0.04$, still deviating substantially from ζ. Independent of the averaging procedure, the enstrophy decay rate showed power-law behavior consistent with the scaling theory, $\Omega(t) \propto t^{-0.36}$.

The results discussed in the previous paragraphs are all based on simulations of the Navier–Stokes equations with Newtonian dissipation replaced by a hyperviscous dissipation operator. Additionally, an investigation based on contour dynamics simulations has been reported [74]. Similar studies based on DNS of freely decaying 2D turbulence of the Navier–Stokes problem, i.e., with Newtonian dissipation, are rather scarce, and the results achieved in this way seem to deviate from the scaling theory put forward by Carnevale et al. [67,68]. The problem with this setup is the slow convergence of the measured decay exponents with increasing initial Reynolds number. Chasnov [75] investigated the asymptotic decay laws of the energy and the enstrophy. By introducing a critical initial Reynolds number, Re_c, Chasnov [75] could

distinguish two different regimes. In case the initial Reynolds number of the flow, defined by $\mathrm{Re}_{\mathrm{ini}}=\mathrm{Re}(t=0)$, is smaller than Re_c, it appears that $\mathrm{Re}(t)\propto E(t)/(\nu\sqrt{\Omega(t)})$ decreases in the course of time. The other regime emerges in the case $\mathrm{Re}_{\mathrm{ini}}>\mathrm{Re}_c$, and the Reynolds number tends to increase in the course of time. The two regimes are separated by $\mathrm{Re}_{\mathrm{ini}}=\mathrm{Re}_c$, and then the Reynolds number remains constant. In that particular case it can be shown for the large-time behavior that $E(t)\propto t^{-1}$ and $\Omega(t)\propto t^{-2}$, and the enstrophy decay rate is in agreement with Batchelor's [15] decay law (but the kinetic energy is not constant, in disagreement with the assumption made by Batchelor [15]). Obviously, for $\mathrm{Re}_{\mathrm{ini}}<\mathrm{Re}_c$ the decay rates of energy and enstrophy are even faster. In the other regime and for increasing initial Reynolds number, it is observed that the power-law exponent of the enstrophy tends to a limiting value: $\Omega(t)\propto t^{-0.8}$, a substantially steeper decay than predicted by the scaling theory (see also recent numerical data by Dmitruk and Montgomery [76]).

Bartello and Warn [77] found $\Omega(t)\propto t^{-1.2}$ for simulations with Newtonian vicosity, although for lower initial Reynolds number (their resolution was 1024^2 collocation points). This result seems consistent with those of Chasnov [75]. Similar studies were conducted by Clercx and co-workers [78–80], although the initial conditions consisted here either of 10×10 slightly perturbed vortices located on a quasiregular grid [78,79] or of a combination of two subsets of 32 vortices [80]. These studies have in common the observation that the long-time behavior of the enstrophy is more or less in agreement with Chasnov's [75] results. Additionally, power-law exponents for, e.g., $\rho(t)$ and $a(t)$ are reported, but it is not clear whether these exponents are affected by the use of Newtonian dissipation instead of hyperviscous dissipation. A systematic study of decaying 2D Navier–Stokes turbulence is needed where the initial Reynolds number (and the resolution) is increased. This is still lacking but is needed to understand if and how Newtonian viscosity might result in modified vortex statistics.

In summary we can conclude that numerical simulations of decaying 2D turbulence employing some form of a hyperviscous dissipation operator provide rather convincing evidence in favor of the scaling theory proposed by Carnevale et al. [67,68]. Not such strong support is found for Batchelor's [15] scaling theory. However, decaying 2D turbulence computations applying Newtonian dissipation do not support either theory, which is, for example, illustrated by the power-law decay of the enstrophy. The decay exponent seems to saturate around the value of 0.8 [75,76], and Reynolds numbers several orders of magnitude larger than currently possible are needed to conclude this issue.

2.3 Quasi-Equilibrium States of Decaying 2D Turbulence. The formation of large-scale vortices and quasistationary final states in quasi-2D turbulence in fluid flows and plasmas has been studied extensively in laboratory experiments and numerical studies. Some of the decaying turbulence simulations revealing the formation of large-scale vortices were already mentioned in Sec. 2.2 [55,57]. Additionally, the work by Matthaeus et al. [81] convincingly showed the self-organization of the flow during the decay process in one large-scale dipolar quasi-equilibrium state. This state is found to be stable and stationary, provided that the Reynolds number is sufficiently high such that the dipolar vortex is subject to very weak dissipation only. Note that under certain conditions also one-dimensional (1D) quasi-equilibrium states have been reported, the so-called "bar" states, instead of the dipole solutions [82]. The prediction of large-scale quasistationary structures has, however, a somewhat longer history. Already 60 years ago Onsager [6] applied the principles of statistical mechanics to predict the appearance of coherent structures by considering a system of point vortices, and the history of the application of statistical mechanics to hydrodynamic turbulence is recently reviewed by Eyink and Sreenivasan [83]. In this section, it is instructive to consider a few of the developments relevant to bounded 2D flows.

An important tool to characterize the quasi-equilibrium late-time states of decaying 2D turbulence is the (ω,ψ) relationship, with ψ as the stream function (with $u=\partial\psi/\partial y$ and $v=-\partial\psi/\partial x$, and x and y as the coordinates in a Cartesian frame of reference). In the absence of viscous dissipation, the steady solutions of the 2D Euler equations are described by $J(\omega,\psi)=(\partial\omega/\partial x)(\partial\psi/\partial y)-(\partial\psi/\partial x)(\partial\omega/\partial y)=0$, or $\omega=f(\psi)$. This immediately yields $\nabla^2\psi=-f(\psi)$, which can in principle be solved with appropriate boundary conditions. A series of simulations by Matthaeus and coworkers [81,84,85] revealed a pointwise hyperbolic sinusoidal relationship between ω and ψ. Such a relation has been predicted in the context of a mean-field treatment of ideal line vortices by Joyce and Montgomery [86,87], who introduced the sinh-Poisson equation for the statistical equilibrium of a point-vortex system. Further extensions and refinements of this theory have been published in later years [88,89]. All these results refer to ideal inviscid systems. Such point-vortex systems are Hamiltonian with finite phase space and can be described by Maxwell–Boltzmann statistics.

Since the late 1980s alternative formulations have been put forward independently [90–93]. The main difference with the point-vortex approach is the introduction of finite-area, mutually exclusive patches of vorticity. This formulation becomes in the limit of zero patch area equivalent with the point-vortex system. These systems can be described by Lynden-Bell statistics.

At this point it might be useful to point out one of the open questions concerning the statistical-mechanical analysis of 2D turbulence: What is the relation of the 2D Navier–Stokes equations to the 2D Euler equations (zero viscosity)? Statistical-mechanical theories for the evolution of 2D turbulent velocity fields, as those mentioned above, make use of nondissipative mean-field models such as ideal line vortices or mutually exclusive convected patches of conserved vorticity. However, any numerical test of the long-term evolution of continuous 2D turbulence will quickly outrun its resolution if no small-scale dissipation of any kind (such as viscosity) is employed to limit the minimum length scale no matter how high the Reynolds number is. All simulations reported on decaying 2D turbulence and run for several eddy turnover times show substantial dissipation of enstrophy. In a recent study, Dmitruk and Montgomery [76] undertook efforts to discover a regime where the Euler behavior would occur for several eddy turnover times by pushing the Reynolds number to the highest possible value. They could not discover a regime where viscous dissipation was insignificant; a significant decay of the enstrophy was observed even for the highest Reynolds number runs with $\Omega(t)\propto t^{-0.8}$ (in agreement with previous studies [75,79]). To find such a regime, if it exists anyway, the Reynolds number should most likely be raised by many orders of magnitude, which is currently, and for the near future, out of reach of computational resources. The inaccessibility of the Euler regime by numerical simulations should always be kept in mind by numerical validation of the statistical-mechanical approaches to predict quasi-equilibrium final states (and, in particular, when no-slip domain boundaries are present).

Quasistationary final states in bounded domains were reported by Montgomery and Joyce [87] (rectangular domain with aspect ratio of 2 and free-slip boundaries), by Pointin and Lundgren [88], and by Ting et al. [89]. Pointin and Lundgren [88] studied the equilibrium statistics of a large number of 2D point vortices of arbitrary sign, evolving in an arbitrary domain closed by a bounded (free-slip) curve. The case of spatially uniform and globally neutral distributions of point vortices (as many positive as negative) in either a square, a rectangular, or a circular domain is of particular interest to 2D bounded turbulence. The solution in a square domain corresponding to the largest value of the entropy is characterized by a single maximum or minimum of the stream function in the center of the domain. Solutions with smaller values of the entropy are characterized by dipolarlike solutions, with the

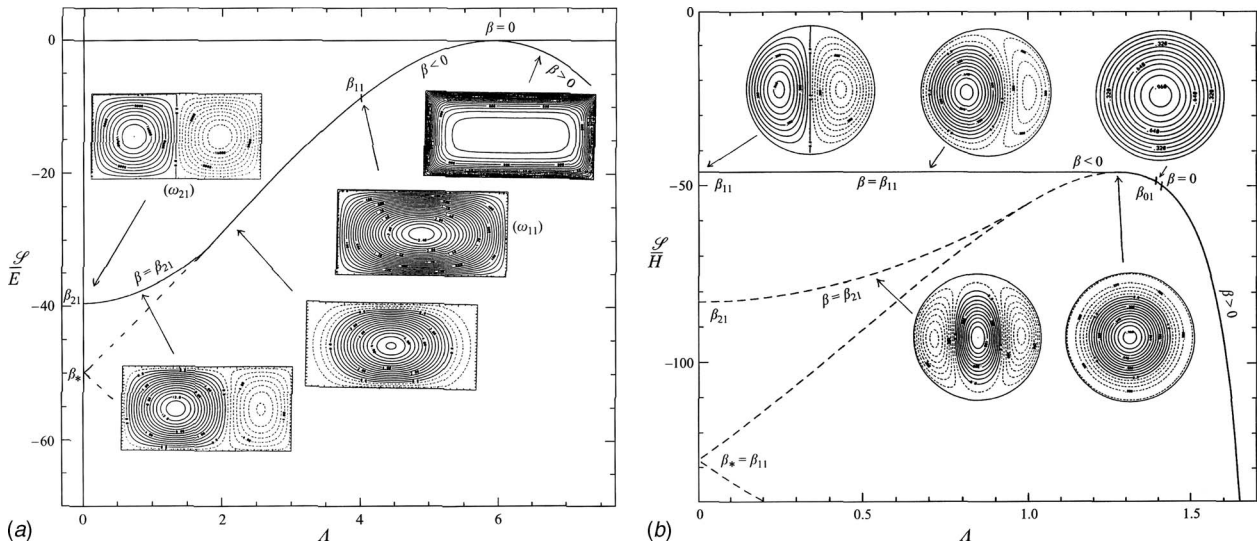

Fig. 4 Entropy of the main modes in (*a*) a rectangular domain with $\delta=2$ and (*b*) a circular domain versus the control parameter Λ. The solution with the highest entropy is along the solid line, and the others are along the dashed line. The dipole solution has in both cases the highest entropy and joins continuously the monopole solution. Courtesy of Chavanis and Sommeria [93].

dipole symmetry line either parallel with the boundary or diagonal in the square domain. In a bounded rectangular domain with aspect ratio $\delta=2$, the solution consists of two cells of opposite circulations, which both fill one-half of the domain [87,88]. A similar prediction was made by Chavanis and Sommeria [93] using a statistical-mechanical theory based on a patchwise discretization of the initial vorticity field. These authors found a monopolar equilibrium solution for a domain with aspect ratio $\delta<1.12$ and a dipolar solution for a domain with $1.12<\delta\leq 2$, provided that the total circulation in the domain, Γ, is zero. For $\Gamma\neq 0$ eventually monopolarlike structures can be found, provided that the control parameter $\Lambda=\Gamma/\sqrt{2E}$ exceeds a critical value. They constructed a diagram of entropy versus the control parameter Λ which is shown in Fig. 4(*a*) for a container with $\delta=2$. Solutions for $\delta>2$ were not described.

Similar studies have been carried out for the circular domain with free-slip boundaries. Here, the angular momentum of the fluid is another constant of the motion that has to be taken into account. The solution with zero angular momentum corresponding to the largest value of the entropy is the dipolar vortex completely filling the disk. Another branch of the solution (with smaller values of the entropy) is the quadrupolar solution, i.e., two positive and two negative vorticity patches each occupying a quadrant of the disk. The maximum-entropy solution with nonzero angular momentum is a domain-filling monopolar vortex [88]. Similar predictions were reported by Chavanis and Sommeria [93], and their regime diagram, shown in Fig. 4(*b*), illustrates the different solutions as a function of the angular momentum and circulation (via a control parameter Λ, which differs from the one introduced above [93]). For the zero angular momentum solution, the dipole is found to have a higher entropy than the corresponding monopole solution, and for Λ sufficiently large a monopolar solution is found. A few lower entropy branches are shown, representing, for example, a tripolar solution.

Since these maximum-entropy solutions do not take into account the effects of viscous boundary layers, the structure of these cell patterns is entirely due to the geometry of the domain. The role of lateral no-slip boundaries on possible "quasistationary" final states will be discussed in Sec. 4.2.

3 Quasi-2D Flows in Shallow Fluid Layers: Laboratory Experiments

Since the mid-1980s many of the theoretical and numerical predictions on (unbounded) 2D turbulence have been put to test with laboratory experiments. Much emphasis has been laid upon measuring the inverse energy and direct enstrophy cascades and associated energy and enstrophy fluxes, the structure functions and PDFs of velocity and vorticity increments, and condensation phenomena. Moreover, vortex statistics of freely evolving 2D turbulence and (eventually) the quasistationary final states have been measured experimentally. Several laboratory techniques exist for generating (quasi-)2D flows. The most popular are rapidly rotating homogeneous fluids, fluids with homogeneous density stratification or two-layer stratification, shallow fluid layers where geometrical confinement is used to acquire a quasi-2D flow, and soap films.

Here we will review in particular the shallow fluid-layer experiments (for a review on soap-film experiments, see Kellay and Goldburg [4]). In these experiments most of the topics mentioned above are addressed. Moreover, several of the shallow fluid-layer experiments reported in the literature address issues directly relevant for laterally bounded 2D turbulence such as vortex statistics, quasistationary final states, vortex-wall interactions, and condensation phenomena. Besides presenting a historical overview, we will briefly discuss some recent shallow fluid-layer experiments [94–101] and those results relevant for understanding laterally bounded 2D turbulence [95,96,99]. In Sec. 4 we will also address several laboratory experiments in stably stratified fluids with direct relevance for bounded 2D turbulence.

3.1 Quasi-2D Turbulence in Shallow Mercury Layers. The first experimental study of the 2D inverse energy cascade was reported by Sommeria [102]. His experimental apparatus [103] consisted of a square box with length of 12 cm containing a mercury layer of thickness of $H=2$ cm. The flow in the horizontal mercury layer was driven electrically. The mercury layer is subjected to a uniform vertical magnetic field to suppress 3D instabilities. For details of the setup and the forcing mechanism, see Sommeria [102]. With the strong magnetic field, two distinct flow regions can be identified in the shallow mercury layer: the core

region where the flow is in good approximation horizontal and uniform (thus 2D) and a thin boundary layer near the horizontal bottom wall (the so-called Hartmann boundary layer). The thickness δ of the boundary layer is estimated as $\delta = H/M$, with $M = HB\sqrt{\sigma/\rho\nu}$ as the Hartmann number (B as the magnetic field strength, σ as the fluid conductivity, ρ as the density, and ν as the kinematic viscosity of mercury). The viscous friction in the Hartmann layer affects the flow in the core. The 2D flow velocity field $\mathbf{u}$ experiences a linear damping [102], $-\mathbf{u}/\tau_M$, with $\tau_M = (1/M) \times (H^2/\nu)$. The flow in the core is therefore described by the following nondimensional equation of motion:

$$\frac{\partial \mathbf{u}}{\partial t} + \mathbf{u} \cdot \nabla \mathbf{u} = -\nabla p + \frac{\nabla^2 \mathbf{u}}{\mathrm{Re}} - \frac{\mathbf{u}}{\mathrm{Re}_M} + \mathbf{F} \tag{15}$$

and $\nabla \cdot \mathbf{u} = 0$. Here, Re is the usual Reynolds number and Re_M is the ratio of the typical time scale of Hartmann friction and the eddy turnover time of the 2D flow. In these experiments $\mathrm{Re} \approx 10^4$ and $1 \lesssim \mathrm{Re}_M \lesssim 40$; thus dissipation is basically due to Hartmann friction ($\mathrm{Re}_M \ll \mathrm{Re}$).

For the experiments with a 6×6 vortex-mode forcing, 1D spectra were measured. For $14 \lesssim \mathrm{Re}_M \lesssim 30$ the spectra contain intervals with a $-5/3$ slope over about half a decade in the best cases. The Kraichnan–Kolmogorov constant C_1 estimated from these experiments fall in the range of 3–7, reasonably close to the value of $C_1 \approx 6$ found in high-resolution numerical simulations. For $\mathrm{Re}_M \lesssim 14$ most of the kinetic energy is drained by Hartmann friction, thus destroying the inverse cascade regime. The absence of the $-5/3$ scaling in the case $\mathrm{Re}_M \gtrsim 30$ might be due to the appearance of a global large-scale circulation cell. This cell might yield departures from homogeneity and isotropy of the turbulent flow. Moreover, this cell interacts with the lateral domain boundaries, although this could not be observed in these experiments due to the limited experimental resolution.

The spontaneous formation of a large-scale circulation cell (with a diameter comparable to the box size) is first observed for $\mathrm{Re}_M \approx 35$. On top of the large-scale circulation cell, smaller eddies can be observed. It is found that either rotation sense is possible. Also disturbances can occur, which destroy the large-scale circulation with a subsequent buildup of a cell with the same or opposite sense of rotation. The time needed for reversal is of the order of a few eddy turnover times but substantially shorter than the average time between two subsequent reversals. These experiments clearly indicate that the probability of reversals decreases with increasing Re_M; for $\mathrm{Re}_M > 41$ no reversals were observed. Note that 2D turbulence without bottom friction is recovered for $\mathrm{Re}_M \to \infty$. A well-defined mechanism for the reversals has not been identified in this study and neither in a numerical simulation of this experiment [104]. This numerical study is based on a simulation of Eq. (15) on a square domain with stress-free boundaries ($\omega = 0$ at the domain boundaries).

Recent high-resolution DNS of forced 2D turbulence (without bottom friction, but a typical forcing scale similar to that used by Sommeria [102]) also revealed the appearance of a large-scale circulation [105]. However, also sudden reversals are observed despite the absence of bottom friction. Moreover, it was revealed that the interaction of the large-scale vortex with the no-slip sidewalls, thus producing small-scale strong vortices, is essential for the occurrence of reversals. A more extensive discussion of these results is postponed to Sec. 4.4.

3.2 Decaying Quasi-2D Turbulence in Shallow Layers of Electrolytes. In the early 1990s a slightly different experiment for the study of 2D turbulence has been proposed by two different groups [70,106,107]. The laboratory experiments have been performed in a shallow layer of electrolyte, in which the motion is generated by electromagnetic forcing. Magnets are placed underneath the fluid layer, and a uniform electrical current runs through the fluid, between two electrodes placed on opposite sidewalls. The interaction of the current density and magnetic field induces a Lorentz force that sets the fluid in motion. Important assumptions to achieve quasi-2D motion in these shallow fluid layers are that horizontal scales of motion are much larger than the fluid-layer thickness (a condition usually achieved by controlling the magnet size and the fluid-layer thickness) and that typical flow velocities are much smaller than the speed of surface waves. However, the quasi-2D flow shows distinct differences compared with the uniform flow in the core of the shallow mercury layer. In order to satisfy the no-slip bottom boundary condition, even a planar flow shows a strong z-dependence resembling a Poiseuille-like profile [108]. The assumption of planar flow with a vertical Poiseuille-like profile allows us to replace $\nu(\partial^2 \mathbf{u}/\partial z^2)$ by $-\lambda \mathbf{u}$, which is known as "Rayleigh friction." The bottom or Rayleigh friction coefficient is $\lambda = \nu(\pi/2H)^2$, with H as the fluid-layer depth (the top and bottom boundary conditions are stress-free and no-slip, respectively). The quasi-2D (Q2D) flow in shallow fluid layers is thus parametrized by

$$\frac{\partial \mathbf{u}}{\partial t} + \mathbf{u} \cdot \nabla \mathbf{u} = -\nabla p + \frac{\nabla^2 \mathbf{u}}{\mathrm{Re}} - \frac{\mathbf{u}}{\mathrm{Re}_\lambda} + \mathbf{F}_L \tag{16}$$

with $\mathbf{F}_L$ as the Lorentz force acting on the fluid and Re_λ as the ratio of the bottom-friction time scale and the eddy turnover time scale of the horizontal flow. It is furthermore assumed that the 2D flow is incompressible; thus $\nabla \cdot \mathbf{u} = 0$. The integral-scale Reynolds number in these experiments [70,106] is usually smaller than in shallow layers of mercury, $\mathrm{Re} \approx 1000-2000$.

This approximation for flows in shallow fluid layers should be considered with care. Introduction of Rayleigh friction assumes horizontal flow in the shallow fluid layer, and in particular for nonstationary flows this is highly questionable. Recent stereoscopic particle image velocimetry (SPIV) measurements of an electromagnetically generated dipolar vortex in a shallow fluid layer show complex 3D velocity fields casting substantial doubt on the validity of Eq. (16) for shallow flows [100,101]. Indirect indications that the flow in shallow fluid layers is not purely 2D were already provided by the experimental study of the free decay of Q2D turbulence by Cardoso et al. [70]. They revealed disagreements with the scaling theory proposed by Carnevale et al. [67,68] (see Sec. 2.2). An initial field of 100 vortices is left to decay, and they found that $\rho(t) \propto t^{-\zeta}$, with $\zeta = 0.44 \pm 0.1$, thus with a distinctly different exponent as proposed by numerical studies ($\zeta \approx 0.72-0.75$). Additionally, the normalized (to take into account bottom friction) vorticity extrema are not conserved. Finally, the scaling theory predicts that the area occupied by the vortices should decrease rapidly, yielding a dilute system of vortices. Cardoso et al. [70] did not observe such an evolution. The flow remained densily filled with vortex clusters. It suggested that the shallow fluid-layer setup does not provide an ideal 2D system.

Based on these observations, an alternative setup has been proposed: the stratified shallow fluid layer [71,109]. The setup is basically the same as for the nonstratified case, but now the cell is filled with two layers of electrolytes with slightly different densities. The heavier fluid is on the bottom, and the flow in this layer is driven by the Lorentz force. The upper layer is lighter and hardly driven by the Lorentz force (the distance to the magnets is relatively large) but by the interfacial stress between the upper and lower layers. For an explanation of the transfer of vorticity from the bottom to the top layer and for an assessment of the relaxation of 3D perturbations in a thin stratified layer of electrolyte, Paret et al. [110] can be consulted. In that paper it was basically concluded that vertical momentum transfer is substantially enhanced by the stratification. Moreover, it was conjectured that for time scales of a typical experiment the flow at the free surface behaves as 2D. The density difference at the interface further acts to suppress vertical velocities.

The quasistationary equilibrium states of 2D turbulence and the scaling theory for the vortex population have been reconsidered

with experiments in these thin stably stratified fluid layers [71,109]. Marteau et al. [109] concluded that the final states of decaying 2D turbulence in square domains disagree with both the statistical [86,87,90,92] and selective decay [55] theories. Marteau et al. [109] concluded that the flow evolution in their experiment is in better agreement with the scaling theory proposed by Carnevale et al. [67,68]. Quite remarkably, similar late-time decay scenarios and final states as those reported by Marteau et al. [109] are observed in decaying 2D turbulence simulations with similar initial integral-scale Reynolds numbers in square domains with no-slip walls [111]. This hints at the possibility of a different interpretation of the experimental results of Marteau et al. [109]. A scaling exponent for the vortex density that is close to the numerical predictions, $\zeta \approx 0.70 \pm 0.1$, has been reported [71], but they needed a change in variables (see Sec. 3.3). Unfortunately, this study also indicated lack of conservation of the (normalized) vorticity extrema. Although it is tempting to conclude that these experiments confirm the scaling theory, it is worthwhile noting that numerical studies of vortex statistics in square containers with no-slip boundaries [78,79,95], starting with initially 100 vortices, predict scaling exponents similar to those reported by Hansen et al. [71], particularly for the intermediate and late-time viscous decay stages. Once again, interpretation of experimental data might be a delicate issue.

First results of an experimental study of the role of lateral no-slip sidewalls on decaying quasi-2D shallow flows in thin stably stratified layers of electrolytes were reported by Wells and Afanasyev [96]. The experimental setup is comparable with the one employed by Hansen et al. [71]. A series of experiments has been conducted to investigate decaying Q2D turbulence in a square and rectangular container and the possible generation of angular momentum due to vortex-wall interactions. The experimental results demonstrate that variations in net angular momentum, defined with respect to the center of the container, occur due to the interaction of dipoles and jets with the lateral no-slip walls of the container. These observations are in agreement with numerical studies of decaying 2D turbulence in square domains with no-slip boundaries [111].

3.3 The Role of Bottom Friction and Fluid-Layer Depth. In most of the experiments discussed in Sec. 3.2, it is assumed that the two-dimensionality hypothesis for such flows holds and that bottom friction can be accounted for with the relatively simple Rayleigh friction model. The validity of these assumptions has been investigated numerically by Satijn et al. [112] for an evolving axisymmetric monopolar vortex in a shallow fluid layer. Paret et al. [110] addressed this issue for decaying Q2D turbulence and claimed that the flow could indeed be considered as 2D after a short initial transient state. A related numerical study of decaying 2D turbulence (with stress-free boundaries) by Jüttner et al. [108] yielded similar conclusions. Although these studies provided important insights in the flow dynamics in shallow fluid layers, conjectures on the quasi-2D behavior of turbulence in shallow fluid layers should be done with care. In recent years more studies have been reported on the influence of the bottom friction and the fluid-layer depth on decaying quasi-2D turbulence [94,95].

The kinetic energy of the 2D flow is defined as $E=\frac{1}{2}\int_{\mathcal{D}}|\mathbf{u}|^2 dA$, and the enstrophy is defined as $\Omega=\frac{1}{2}\int_{\mathcal{D}}\omega^2 dA$. A relation between the energy decay rate and the enstrophy is easily derived from Eq. (16),

$$\frac{dE(t)}{dt} = -\frac{2}{\mathrm{Re}}\Omega(t) - \frac{2}{\mathrm{Re}_\lambda}E(t) \tag{17}$$

where time has been made dimensionless with the ratio of the box size over the root-mean-square (rms) velocity of the initial horizontal flow. By introducing the following expressions for the energy and the enstrophy:

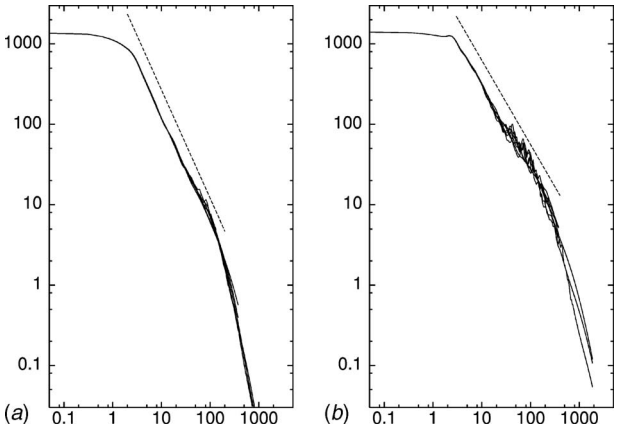

Fig. 5 Time evolution of the compensated enstrophy $\Omega_0(\tau)$ for (*a*) Re=2000 and (*b*) Re=5000, with $\mathrm{Re}_\lambda \in \{10,20,25,33.3,50,100,\infty\}$. The dashed lines indicate power laws (*a*) $\tau^{-1.35}$ and (*b*) $\tau^{-1.05}$. Both figures are taken from Clercx et al. [95].

$$E(t) = E_0(t)e^{-2t/\mathrm{Re}_\lambda}, \quad \Omega(t) = \Omega_0(t)e^{-2t/\mathrm{Re}_\lambda} \tag{18}$$

with $E_0(t)$ and $\Omega_0(t)$ independent of the bottom friction, Eq. (17) becomes

$$\frac{dE_0(t)}{dt} = -\frac{2}{\mathrm{Re}}\Omega_0(t) \tag{19}$$

Apparently, $E_0(t)$ and $\Omega_0(t)$ can be considered as an energy and an enstrophy, respectively, of a 2D flow without bottom friction and are therefore denoted as the compensated kinetic energy and the compensated enstrophy of the flow, respectively. Moreover, it indicates that we might introduce the following relations for the velocity and the vorticity: $\mathbf{u}(x,y,t)=\mathbf{u}_0(x,y,t)e^{-t/\mathrm{Re}_\lambda}$ and $\omega(x,y,t)=\omega_0(x,y,t)e^{-t/\mathrm{Re}_\lambda}$. Note that x, y, and t are all dimensionless.

The ratio $\Omega(t)/E(t) \propto 1/l^2$ provides an estimate of the average length scale l in the flow. Applying the relations from Eq. (18), we obtain $\Omega(t)/E(t)=\Omega_0(t)/E_0(t)$, and l should therefore be independent of the bottom friction.

Hansen et al. [71] introduced a procedure to simplify the vorticity equation,

$$\frac{\partial\omega}{\partial t} + (\mathbf{u}\cdot\boldsymbol{\nabla})\omega = \frac{1}{\mathrm{Re}}\boldsymbol{\nabla}^2\omega - \frac{1}{\mathrm{Re}_\lambda}\omega \tag{20}$$

Substituting $\omega=\omega_0 e^{-t/\mathrm{Re}_\lambda}$ and $\mathbf{u}=\mathbf{u}_0 e^{-t/\mathrm{Re}_\lambda}$ in Eq. (20), subsequently multiplying by $e^{t/\mathrm{Re}_\lambda}$, and rescaling time to $t_*=\mathrm{Re}_\lambda(1-e^{-t/\mathrm{Re}_\lambda})$, we arrive at the following modified vorticity equation [113]:

$$\frac{\partial\omega_0}{\partial t_*} + (\mathbf{u}_0\cdot\boldsymbol{\nabla})\omega_0 = \frac{1}{\mathrm{Re}_*}\boldsymbol{\nabla}^2\omega_0 \tag{21}$$

with $\mathrm{Re}_*=\mathrm{Re}\, e^{-t/\mathrm{Re}_\lambda}$ (or $\nu_*=\nu e^{t/\mathrm{Re}_\lambda}$). The approach introduced by Hansen et al. [71] implies that 2D flows with bottom friction can be interpreted as purely 2D flows without bottom friction, but with a time-dependent horizontal Reynolds number, which can evolve for a finite time t_* ($\leq \mathrm{Re}_\lambda$) only.

The validity and limitations of this approach have been discussed recently [95] based on a comparison of numerical data from several decaying 2D turbulence runs with different values of the bottom friction and initial integral-scale Reynolds numbers of 1000, 2000, and 5000. The compensated enstrophy is shown in Fig. 5 for Re=2000 (left panel) and Re=5000 (right panel) [114]. These plots clearly show the bottom-friction independence of $\Omega_0(\tau)$; the curves for the different values of Re_λ are hardly distin-

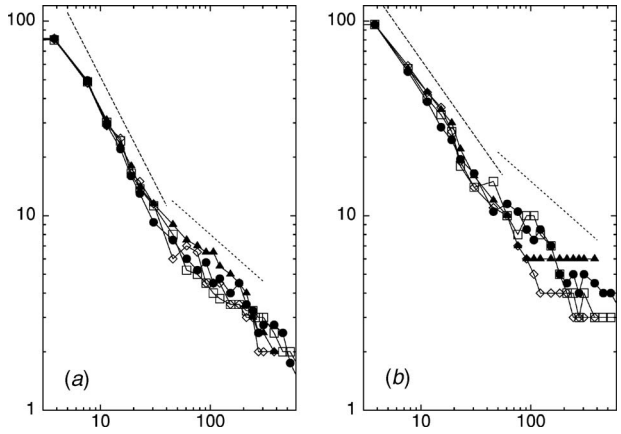

Fig. 6 Time evolution of the average vortex density $\rho(\tau)$ for (*a*) Re=2000 and (*b*) Re=5000. Filled circles, $\mathrm{Re}_\lambda=\infty$; open squares, $\mathrm{Re}_\lambda=50$; open diamonds, $\mathrm{Re}_\lambda=20$; filled triangles, $\mathrm{Re}_\lambda=10$. The dashed lines indicate power laws (*a*) $\tau^{-1.10}$ and (*b*) $\tau^{-0.80}$ for $\tau\lesssim 50$. Late-time power laws are approximated by $\tau^{-0.50}$. Both figures are taken from Clercx et al. [95].

guishable (note that the fluctuations for $\tau\gtrsim 40$ in the right panel are due to vortex-wall interactions generating enstrophy). Moreover, for $\tau\lesssim 100$ power-law behavior is found, $\Omega_0(\tau)\propto\tau^{-\beta}$, with $\beta=1.35\pm0.10$ for Re=2000 and $\beta=1.05\pm0.10$ for Re=5000. These simulations, moreover, showed that the evolution of vortex statistics of decaying 2D turbulence with bottom friction can be described by bottom-friction independent power laws (provided that compensated velocity and vorticity fields are used); see Fig. 6 for the average vortex density. For both Re=2000 and Re=5000, two different power-law regimes can be identified for $\rho(\tau)$. The simulations with Re=2000 revealed that $\rho(\tau)\propto\tau^{-1.1}$ for $\tau\lesssim 50$ and $\rho(\tau)\propto\tau^{-0.5}$ for $\tau\gtrsim 50$ (see Fig. 6(*a*)). The data obtained for the runs with Re=5000 revealed $\rho(\tau)\propto\tau^{-0.8}$ for $\tau\lesssim 60$ and $\rho(\tau)\propto\tau^{-0.5}$ for $\tau\gtrsim 60$ (see Fig. 6(*b*)). The rescaling of time ($t\rightarrow t_*$) proposed by Hansen et al. [71] does not modify power-law exponents for $t\lesssim \mathrm{Re}_\lambda$ (the same power laws are necessarily found), and for $t\gtrsim \mathrm{Re}_\lambda$ any clear power-law behavior is absent, even if the rescaled time t_* is introduced. In the latter regime the computed data show strong bottom-friction dependence and are strongly dominated by lateral diffusion. The introduction of the rescaled time t_* appears to be rather ineffective for the present range of Reynolds numbers.

A series of laboratory experiments have also been conducted for various fluid-layer depths [95]. For several fluid depths ($H\geq 8$ mm), similar decay rates have been found for the compensated energy $E_0(t)$ and enstrophy $\Omega_0(t)$. It is, for example, found that $\Omega_0(t)\propto t^{-1.0\pm0.1}$, similar to the numerically obtained power-law. For this range of fluid-layer depths, the power-law dependence could clearly be separated from the exponential decay due to bottom friction. The observed decay rates for $\Omega_0(t)$ and $\Omega_0(t)/E_0(t)$ are consistent with those obtained earlier [94] (although this study was performed with shallower fluid layers with thicknesses ranging from 2 mm to 6 mm). The experimental power-law exponents of $\rho(t)$, $a(t)$, and $\omega_{\mathrm{ext}}(t)/\sqrt{E(t)}$, measured in experiments with $H\leq 8$ mm, agree remarkably well with those reported by Cardoso et al. [70]. These experiments [95] show that the temporal evolution of coherent vortices and the power-law regimes of integral quantities such as $\Omega(t)/E(t)$ are relatively unaffected by the fluid-layer depth for $H\lesssim 12$ mm. The apparent independence of these quantities from the fluid-layer depth might indicate that they are relatively insensitive to residual 3D flows in shallow fluid layers.

3.4 Forced 2D Turbulence in Thin Stably Stratified Fluids. Experiments with electromagnetically driven flow in a cell with size of 15×15 cm^2, using thin stably stratified layers of electrolytes, also provide evidence of a stationary 2D inverse cascade [115,116]. The typical forcing scale is approximately 15 mm (corresponding to the size of the magnets). The imposed current is a time series of impulses of constant amplitude and random sign and favors homogeneity of the flow. In a two-layer system with a total fluid-layer thickness of 5.5 mm (the bottom friction in the lower layer is large enough to provide an infrared energy sink necessary to avoid accumulation of energy on scales comparable with the box size), the kinetic energy spectrum shows indeed a $k^{-5/3}$ slope, but once again its extent is not more than half a decade (like in the experiments by Sommeria [102] reviewed in Sec. 3.1). The Kolmogorov constant measured in these experiments, $C_1=6.5\pm1$, is consistent with data from numerical studies. In a separate experiment with a total fluid-layer thickness of 7.5 mm, thus reducing the impact of bottom friction, the condensation regime is observed [116] (this condensation phenomenon is also observed recently in a similar experiment [99]).

The study by Paret and Tabeling [116] also considered the statistical properties of velocity differences $\delta\mathbf{u}(\mathbf{x},\mathbf{r},t)=\mathbf{u}(\mathbf{x}+\mathbf{r},t)-\mathbf{u}(\mathbf{x},t)$ (with size of the separation vector $\mathbf{r}$ in the inverse energy cascade range). For statistically stationary flows, it is allowed to drop the time dependence; we are thus left with $\delta\mathbf{u}(\mathbf{x},\mathbf{r},t)=\delta\mathbf{u}(\mathbf{x},\mathbf{r})$. The velocity difference can be decomposed in components parallel and perpendicular to $\mathbf{r}$: $\delta u_\parallel(\mathbf{x},\mathbf{r})=\delta\mathbf{u}(\mathbf{x},\mathbf{r})\cdot\mathbf{r}/r$ and $\delta u_\perp(\mathbf{x},\mathbf{r})=\delta\mathbf{u}(\mathbf{x},\mathbf{r})\cdot\mathbf{r}_\perp/r$, respectively, with $r=|\mathbf{r}|$ and $\mathbf{r}_\perp=\hat{\mathbf{k}}\times\mathbf{r}$ (with $\hat{\mathbf{k}}=(0,0,1)$ as the unit vector perpendicular to the plane of the flow). By assuming homogeneity and isotropy, we can unambiguously drop the $\mathbf{x}$ dependence and replace $\mathbf{r}$ by r in statistical averages; thus, for example, the following notation will be used [117]: $\langle|\delta u_\parallel(\mathbf{x},\mathbf{r})|^n\rangle=\langle|\delta u_\parallel(r)|^n\rangle$. The structure functions of different orders for the longitudinal and transverse velocity components are $S_n^\parallel(r)=\langle|\delta u_\parallel(r)|^n\rangle$ and $S_n^\perp(r)=\langle|\delta u_\perp(r)|^n\rangle$, respectively. Paret and Tabeling [116] were interested in deviations from the classical Kolmogorov result $\langle|\delta u(r)|^n\rangle\sim\epsilon^{n/3}r^{n/3}=(\epsilon r)^{\zeta_n}$, with ϵ as the dissipation rate of energy. Their main conclusion is that intermittency is absent in the inverse energy cascade. The structure functions $S_n^\parallel$ and $S_n^\perp$ are both within experimental accuracy equal to their Kolmogorov values, $\zeta_n=n/3$. Moreover, the statistics of velocity increments is found to be very close to Gaussian. A combined numerical and experimental investigation by Dubos et al. [118] and numerical simulations by Boffetta et al. [28] confirm a nearly Gaussian behavior of the velocity increments. All these studies indicate the absence of any measurable intermittency corrections in the scaling laws for the inverse energy cascade.

In an experimental setup similar to that employed by Hansen et al. [71], Paret et al. [110], and Paret and Tabeling [116], the vorticity statistics in the direct enstrophy cascade has been investigated [119]. In order to obtain a direct enstrophy cascade with a sufficient inertial range, it is necessary to introduce large-scale electromagnetic forcing. The square region was divided into diagonal sectors, thus forming four triangular aggregates. Each triangular aggregate contains approximately 100 randomly distributed small magnets with the same magnetic orientation. Opposite sectors had like polarity. By imposing an unsteady current (nonperiodic, zero-mean, square waveform), the formation of quasipermanent large-scale vortical structures, which might break the self-similarity, is avoided. With this experimental setup, it was possible to obtain a clear $k^{-3.0\pm0.2}$ inertial range over nearly 1 decade. The enstrophy flux η is positive but clearly not constant in the inertial range (maximum enstrophy flux for large wave numbers far away from the forcing scale). With the enstrophy flux averaged over the interval between forcing scale and the maximum wave number, they computed $C_2\approx 1.4\pm0.3$. Rather surprisingly, this value is in very good agreement with the numerical

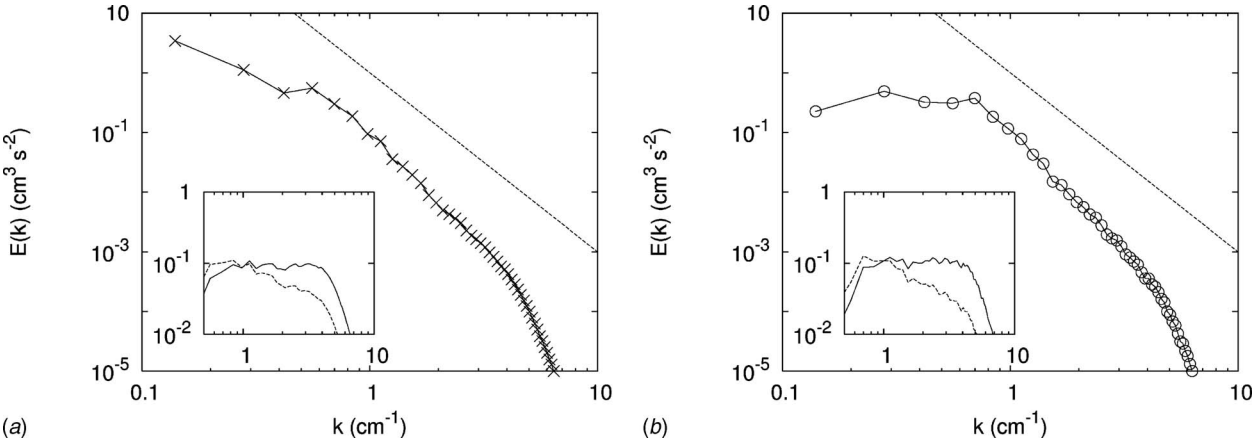

Fig. 7 Kinetic energy spectrum for the experiments with top-layer thickness of (*a*) 6 mm and (*b*) 5 mm. The dashed line in each panel represents the k^{-3} prediction. In the respective insets, the spectrum compensated with $k^{-3-\chi}$ (solid line) and with the Kraichnan prediction k^{-3} (dashed line). In (*a*) $\chi \simeq 0.8 \pm 0.1$, and in (*b*) $\chi \simeq 1.0 \pm 0.1$. Courtesy of Boffetta et al. [98].

result obtained by Borue [35], $C_2 \approx 1.5-1.7$ (note that in these simulations η was constant over approximately 2 decades). The distributions of vorticity increments $\delta\omega(\mathbf{x},\mathbf{r}) = \omega(\mathbf{x}+\mathbf{r}) - \omega(\mathbf{x}) = \delta\omega(r)$ (assuming stationarity, homogeneity, and isotropy of the turbulent flow) in the inertial range deviate hardly from Gaussianity. The structure functions $S_n = \langle |\delta\omega(r)|^n \rangle \propto r^{\zeta_n}$ have exponents hardly distinguishable from zero within experimental uncertainty. This study thus indicates that no substantial small-scale intermittency exists. It should be said here that recent numerical studies [46] and soap film experiments [47] provide evidence for r-dependent scaling of the second-order vorticity structure function. The results by Paret et al. [119] are, within their experimental accuracy, not in disagreement with theoretical predictions of ζ_n for steady 2D turbulence (with r in the direct cascade range) [120,121]. Falkovich and Lebedev [120] showed that $\zeta_n \approx 0$ for all n (with logarithmic corrections, which does not imply that the vorticity structure function should be independent of r; see also measurements of S_2 by Rivera et al. [47]). Eyink [121] obtained $\zeta_2 \leq 2/3$ and $\zeta_n \leq 0$ for $n \geq 3$. Note that the experimental data for S_2 disagree with the prediction by Tran and Bowman [42] who showed for monoscale forcing that $\zeta_2 > 2$ (see also Sec. 2.1).

The role of bottom friction on 2D turbulence and on the scaling of the direct enstrophy cascade has been addressed recently once again experimentally by Boffetta et al. [98]. The experimental setup, including the forcing procedure and distribution of magnets below the tank, is a similar but upscaled version of the one used by Paret et al. [119]. The container has a size of 50×50 cm^2 and is filled with fresh water on top of a bottom layer of 3 mm thickness with an electrolyte solution of water and NaCl. The thickness of the top layer was varied between 3 mm and 7 mm. The injection scale is 9 cm, which yields for the forcing wave number $k_f \simeq 0.7$ cm^{-1}. An inertial range with power-law scaling is found for the wave number range 0.7 cm$^{-1} \leq k \leq 4.0$ cm^{-1}. These experiments indeed revealed a spectral slope in the direct enstrophy cascade range that depends on the thickness of the fluid layer, viz., $k^{-3-\chi}$, with $\chi > 0$ as a correction factor dependent on the bottom friction. For the different heights of the top layer (7 mm, 6 mm, and 5 mm), they found the corrections $\chi \simeq 0.5 \pm 0.1$, 0.8 ± 0.1, and 1.0 ± 0.1, respectively. The kinetic energy spectra and their respective compensated spectra are displayed in Fig. 7. These observations are in agreement with a theoretical prediction by Nam et al. [122] and an earlier numerical work by Boffetta et al. [123]. Similar corrections to the inertial range scaling of the direct enstrophy cascade have been reported for forced 2D turbulence simulations with Rayleigh damping in bounded square domains [124]. It is noteworthy that such steepening of the spectrum has not been reported by Paret et al. [119].

Recently, an important modification of the setup introduced by Hansen et al. [71] and Tabeling and co-workers [110,116] has been proposed by Rivera and Ecke [97]. Usually a stably stratified configuration is used with two thin layers of electrolytes on top of each other (or a layer of fresh water on top of an electrolyte layer). The forcing of the flow occurs basically in the bottom layer. In the setup proposed by Rivera and Ecke [97], the salt water layer floats on a 3 mm layer of Fluorinert FC-77, a dielectric fluid that is immiscible with water. Fluorinert FC-77 has a density that is approximately 1.8 times larger than the density of water and serves as a lubricant between the water layer and the bottom of the container. Obviously, the forcing of the flow now occurs in the top layer of salt water (all the current flows through the salt water since Fluorinert FC-77 is a strong dielectric). They found that the use of Fluorinert FC-77 results in a more strongly stratified flow without significantly modifying the Rayleigh friction. The increased stratification reduces vertical mixing and thus allows stronger forcing. With this modification substantially higher Reynolds numbers can be achieved. It is claimed by Rivera and Ecke [97] that $\mathrm{Re}_s = U l_f / \nu \approx 500$ and $\mathrm{Re}_l = U / l_f \lambda \approx 20$, with l_f as the typical forcing scale ($l_f \ll L$). These are substantially larger than those obtained from the experiments by Paret and Tabeling [115,116], which were estimated as $\mathrm{Re}_s \approx 100$ and $\mathrm{Re}_l \approx 5$. The setup employed by Rivera and Ecke [97] allows measurements of 2D turbulence with simultaneous ranges of the direct enstrophy and inverse energy cascades where both cascades are then separated by a well-defined spatial injection scale, which is determined by the magnet size. Thus far, only a few experimental results using this particular setup have been reported, one on pair dispersion in 2D turbulence [97], a topic not included in this review, and another one focusing on experimental validation of the physical mechanism of the 2D inverse energy cascade put forward by Chen et al. [29] (see Sec. 2.1). They particularly measured the energy spectra (see Fig. 1(*b*)) and instantaneous snapshots of filtered energy fluxes.

3.5 On 3D Structures of Vortices in Shallow Fluid Layers. The assumption of quasi-two-dimensionality of flows in shallow fluid layers and modeling of the influence of the no-slip bottom by imposing Rayleigh friction are mostly based on indirect observations [110] and comparison of numerical simulations of, for example, Eq. (16) with experimental data [95,108]. The laboratory experiments discussed in Secs. 3.1, 3.2, and 3.4 provide ample but indirect evidence in favor of these assumptions. However, the above described assumptions on the behavior of the flow in a shallow fluid layer have never been validated by direct measure-

ments. On dimensional grounds, it is expected that vertical velocities are present and that on average $w \approx (H/L)U$, with w as the vertical velocity component, U as the typical horizontal velocity, and H/L as the aspect ratio of the typical vertical and horizontal length scales in the flow. The source of the three-dimensionality of the fluid motion remains, however, unclear. Possible causes might be the vertical variation in the horizontal flow field due to the no-slip bottom boundary condition, the confinement of the flow, and free-surface deformations. Additionally, it should be realized that the strength of the electromagnetic forcing decays over a limited vertical distance (and the Lorentz force also has a vertical component).

The numerical study by Satijn et al. [112] addressed the decay of an axisymmetric monopolar vortex in a shallow fluid layer. The horizontal Reynolds number associated with the vortical motion is defined by $\mathrm{Re} = UL/\nu$, with U and L as the typical velocity and length scales of the vortex. This investigation focused on the structure and the strength of 3D recirculating flows and in providing a $(\mathrm{Re}, \mathrm{Re}_\lambda)$ regime diagram distinguishing the regimes of Q2D and 3D flow behaviors. Two separate cases have been considered: a vortex in a single shallow layer and a vortex in a thin stably stratified two-layer fluid. A no-slip bottom boundary condition and a rigid stress-free top boundary condition have been applied. For the two-layer fluid, a continuous stress boundary condition has been applied at the further nondeformable interface. It was shown that an axisymmetric vortex in a shallow fluid layer behaves as quasi-2D, provided that the flow is characterized by sufficiently small horizontal and vertical Reynolds numbers [112]: $\mathrm{Re} \lesssim 2000$ and $\mathrm{Re}_\lambda = U/\lambda L = (2H/\pi L)^2 \mathrm{Re} \lesssim 20$. For a thin stably stratified fluid layer, the regime diagram is similar as for the single-layer case, although the condition for Re_λ is somewhat relaxed for the smaller horizontal Reynolds numbers.

By means of SPIV measurements and full 3D simulations of the evolution of a dipolar vortex in a shallow fluid layer, deeper insight in the three-dimensionality of such (dipolar) flows is gained [100,101]. A series of laboratory experiments has been performed in a shallow layer of electrolyte of approximately 6, 9, and 11 mm in a 52×52 cm^2 tank. One disk-shaped permanent magnet (with a diameter of 25 mm) is placed in the center of the tank below the 1 mm thick bottom of the tank. Two rectangular-shaped electrodes are placed on opposite sides of the tank, leading to a uniform current density. A current pulse of 1 s is applied, and a dipolar vortex is generated above the magnet and its evolution is measured afterward. Two cameras, placed at an angle, enable the use of SPIV to measure the full three-component velocity field in a horizontal plane inside the fluid layer. A dual pulse Nd:YAG (yttrium aluminum garnet) laser is used to produce a horizontal light sheet of 1 mm thickness. The fluid is seeded with polystyrene particles having a mean diameter of 20 μm. Three-component velocity fields are measured in horizontal planes near the no-slip bottom, halfway the fluid layer, and just below the free surface. Further technical details can be found elsewhere [100,101].

The SPIV measurements show significant and complex 3D structures, and vertical motions occur throughout the flow evolution, during and after the forcing phase. Comparison with full 3D simulations of these experiments (with the same parameter settings) with either no-slip or stress-free boundary conditions at the bottom revealed that it is not particularly the bottom friction that is responsible for the significant 3D flow but mainly the confinement of the flow (in particular, the impermeability of the bottom boundary). Apparently, the confinement of the flow induces sufficient vertical variation in the horizontal velocity field that strong 3D motions can be supported. Vertical slices of the velocity field also show that any Poiseuille-like vertical variation of the velocity field is absent, also during the decay of the dipole long after the forcing has stopped.

For the case of a flow with stress-free bottom and surface boundary conditions, it is anticipated from the study reported by Akkermans et al. [101] that 3D flow recirculation is absent. Moreover, a forcing mechanism is needed that has no vertical component, with its horizontal component uniform over the fluid height, and that introduces a horizontal divergence-free velocity field. This is a situation that is certainly hard to achieve in practice.

These observations do not invalidate the laboratory experiments of electromagnetically forced flows in shallow fluid layers as reviewed in this section. On the contrary, these experiments, in particular those from 10 to 15 years ago by Tabeling and co-workers [71,106,108–110,115,116,119], even played an important role in pushing the numerical and theoretical research back in the framework of the classical KLB theory of 2D turbulence. However, what can be learned for unsteady flows is the following: Imposing a parametrization of bottom friction provides only a very qualitative description of the influence of 3D motions and does not cover all sources of it. The presence of 3D recirculating flows should preferably not be assessed by global measures such as the averaged horizontal divergence. Finally, in view of the results presented for a single shallow layer, it seems worthwhile to analyze both experimentally and numerically the presumed superior two-dimensionality properties of thin stably stratified fluid layers.

4 2D Turbulence on Confined Domains

As can be concluded from Sec. 2, most numerical investigations of 2D turbulence have been carried out with pseudospectral codes on a square domain subject to double-periodic boundary conditions. While decaying turbulence on a double-periodic square domain eventually becomes organized in the form of a combination of two cells of positive and negative circulations (see Matthaeus et al. [81]), the "final state" of decaying turbulence on a square domain with no-slip boundaries consists of a single large central cell with either positive or negative circulation, surrounded by a shielding ring of opposite vorticity (such that the total circulation of the flow is zero, as dictated by the no-slip boundary condition) [111]. A typical example of the evolution of decaying 2D turbulence with $\mathrm{Re} = 2000$ in a square bounded domain (typical of laboratory experiments in stratified fluids) is shown in Fig. 8. Although the quasistationary final state has not been reached yet, a large central vortex is already visible in the center of the domain. This long-time behavior has been observed in laboratory experiments [126] and also in high-Reynolds number simulations of decaying 2D turbulence in square bounded domains [79].

A remarkable observation was that in many cases the total angular momentum $L(t) = \int_{\mathcal{D}} (xv - yu) dx dy$ of the flow (being randomly initialized, with $L(t=0) = L_0 \simeq 0$; the origin $(x,y) = (0,0)$ of the Cartesian coordinate frame is located in the center of the domain) shows a sudden change to nonzero values—a feature termed "spontaneous spin-up." Illustrations of this phenomenon from both laboratory experiments and numerical simulations have been displayed in Fig. 9. This spin-up of the fluid is directly associated with the self-organization of the flow into a single larger vortex structure [79,127]. In the next stage of the flow evolution, the absolute angular momentum $|L(t)|$ shows a very slow decay to zero for very late times. It is important to note that the no-slip boundary condition is a prerequisite for the spin-up, as the angular momentum $L(t)$ is an irrelevant quantity for the flow evolution on a double-periodic domain. Also, the square domain geometry is important, spin-up being virtually absent on a circular domain or on a long rectangular domain in which the final state consists of a linear (domain-filling) array of counter-rotating cells [128]. Obviously, the change in the total angular momentum during the spontaneous spin-up is connected with the action of forces at the domain boundaries. Numerical simulations have revealed that—for the case of a square geometry—the contribution of the inviscid normal stress (i.e., the pressure) is much larger than the effects of viscous shear and normal stresses.

The above studies were not the first that addressed in a systematic way the role of rigid walls on the evolution of 2D turbulence. Approximately a decade ago, numerical computations of decaying 2D turbulence in a circular geometry with a rigid boundary by Li

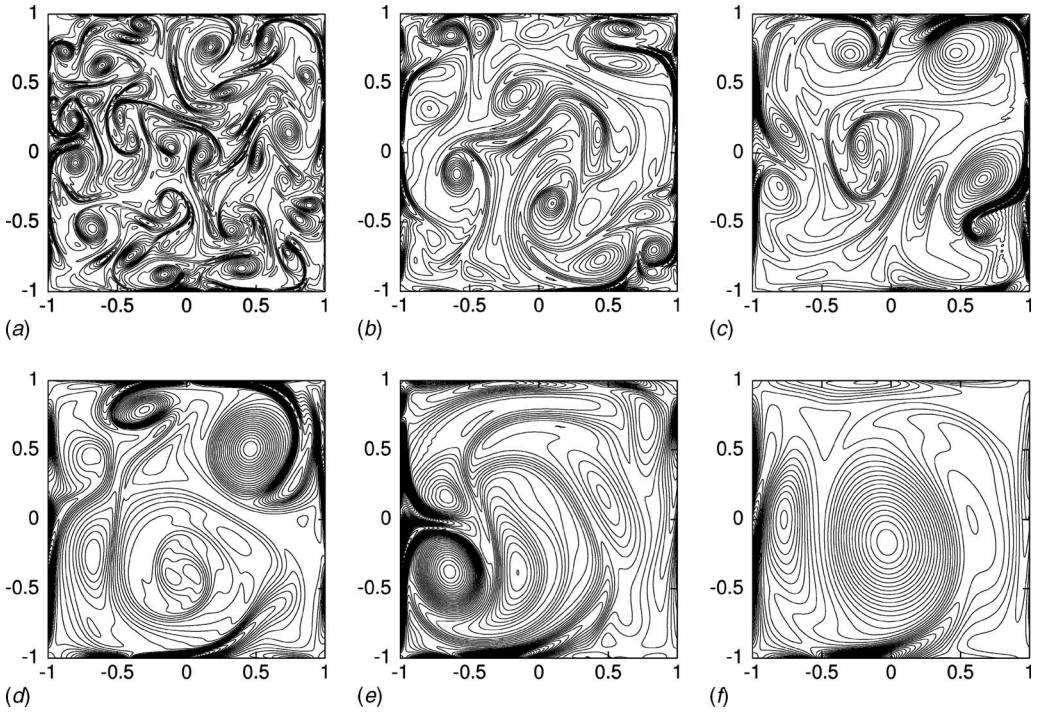

Fig. 8 Sequence of vorticity contour plots for decaying 2D turbulence on a square domain with no-slip boundaries. The flow was initialized by a slightly disturbed array of 10×10 vortices with alternating sense of rotation, with Re=2000. The contour level increments are (*a*) 3, (*b*) 1.5, (*c*) 0.8, (*d*) 0.4, (*e*) 0.2, and (*f*) 0.1. This figure is taken from van Heijst et al. [125].

and Montgomery [129] and Li et al. [130,131] have revealed some remarkable results, which will briefly be discussed in Sec. 4.2.

The 2D motion of an incompressible viscous fluid on a bounded domain $\mathcal{D}$ is conveniently described in a Cartesian frame of reference, with $\mathbf{r}=(x,y,0)$ as the coordinates in the plane of the flow. For the case of a Newtonian fluid, the motion is governed by the Navier–Stokes equation. Solutions of this equation have to satisfy the no-slip and impermeability conditions imposed by the domain boundary, i.e., $\mathbf{u}=0$ on $\partial\mathcal{D}$.

In order to understand the global behavior of the confined flow, it is useful to describe the flow in terms of integral quantities. We already introduced an important global quantity of the flow, the total angular momentum L, which is defined with respect to the domain center,

$$L=\int_{\mathcal{D}}\hat{\mathbf{k}}\cdot(\mathbf{r}\times\mathbf{u})dA=-\frac{1}{2}\int_{\mathcal{D}}r^2\omega dA \tag{22}$$

Here, $\hat{\mathbf{k}}=(0,0,1)$, the unit vector perpendicular to the plane of flow. An expression for its rate of change is derived by taking the time derivative and inserting the Navier–Stokes equation in the

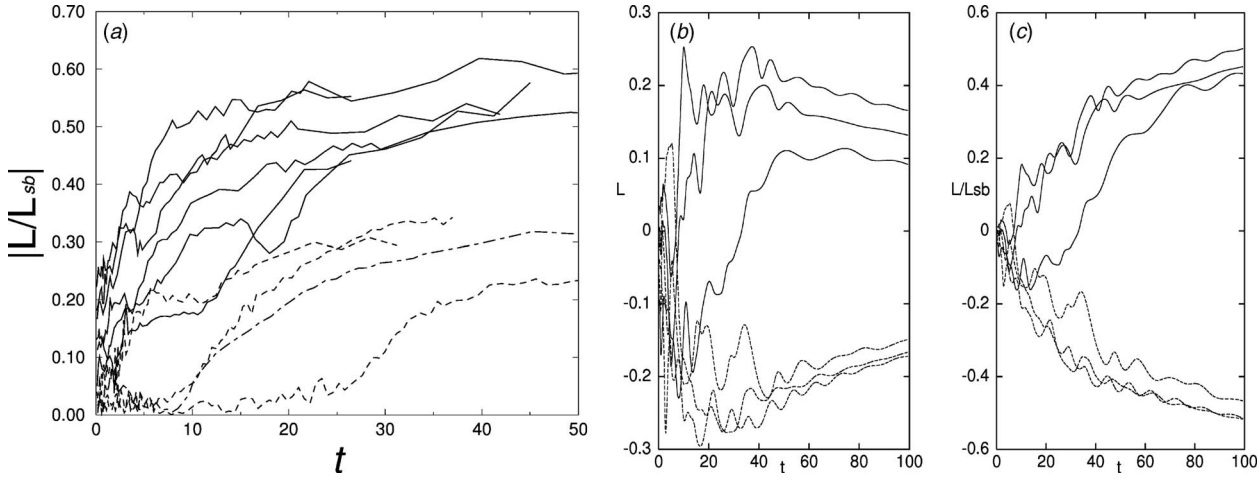

Fig. 9 (*a*) Graphical representation of the normalized net angular momentum $L(t)/L_{sb}(t)$ found in a number of experiments of decaying 2D turbulence. The initial states are characterized by $L_0\approx 0$ (dashed and dashed-dotted lines) and $|L_0|>0$ (solid lines). (*b*) The angular momentum $L(t)$ for six runs from numerical simulations as in Fig. 8, and (*c*) the normalized angular momentum $L(t)/L_{sb}(t)$ for these runs. These figures are taken from van Heijst et al. [125].

integral. For a flow on a domain enclosed by a no-slip boundary, one thus obtains

$$\frac{dL}{dt} = \oint_{\partial\mathcal{D}} p\mathbf{r}\cdot d\mathbf{s} + \frac{1}{\mathrm{Re}}\oint_{\partial\mathcal{D}} \omega(\mathbf{r}\cdot\hat{\mathbf{n}})ds + M(t) \tag{23}$$

or, by using the second integral in Eq. (22) and substituting the vorticity equation,

$$\frac{dL}{dt} = -\frac{1}{2\,\mathrm{Re}}\oint_{\partial\mathcal{D}} r^2\frac{\partial\omega}{\partial n}ds + \frac{1}{\mathrm{Re}}\oint_{\partial\mathcal{D}} \omega(\mathbf{r}\cdot\hat{\mathbf{n}})ds + M(t) \tag{24}$$

where $M(t)=-\frac{1}{2}\int_{\mathcal{D}} r^2 Q(\mathbf{r},t)dA$ represents the net torque introduced by the forcing. Furthermore, $\hat{\mathbf{n}}$ is the unit vector normal to the boundary, $\partial/\partial n$ denotes the normal derivative with respect to the boundary $\partial\mathcal{D}$, and $d\mathbf{s}$ represents an infinitesimal tangential element of the boundary $\partial\mathcal{D}$ (and ds is its length).

Several physical processes that determine the time dependence of the angular momentum are clarified by both formulations of dL/dt, as shown in Eqs. (23) and (24). Obviously, in the unforced case ($M=0$) the change in angular momentum is entirely due to the action of torques of boundary forces associated with the pressure (normal stress) and viscous stresses (normal and shear stress). Note that a circular domain forms a special case because the torque of the normal wall stress is identically zero then. It follows from Eqs. (23) and (24) that the pressure contribution should be proportional to the normal vorticity gradient integrated over the boundary [132]. It is interesting to note that the product $(1/\mathrm{Re})\times(\partial\omega/\partial n)$ should be finite for vanishing viscosity (or $\mathrm{Re}\to\infty$), thereby assuming that the pressure contribution is finite in this limiting case. An immediate consequence is the following scaling behavior of the normal vorticity gradient at the boundary: $\partial\omega/\partial n \propto \mathrm{Re}$.

Other global quantities that are useful in characterizing the flow are the kinetic energy E and the enstrophy Ω. For flows in confined domains with no-slip walls, the evolution of E and Ω is given by

$$\frac{dE}{dt} = -\frac{1}{\mathrm{Re}}\int_{\mathcal{D}} \omega^2 dA = -\frac{2}{\mathrm{Re}}\Omega \tag{25}$$

which is equivalent to the time rate of change of kinetic energy in 2D periodic or unbounded domains, and

$$\frac{d\Omega}{dt} = -\frac{1}{\mathrm{Re}}\int_{\mathcal{D}} |\nabla\omega|^2 dA + \frac{1}{\mathrm{Re}}\oint_{\partial\mathcal{D}} \omega(\hat{\mathbf{n}}\cdot\nabla\omega)ds \tag{26}$$

Here, it is clear that the time rate of change in the enstrophy contains a boundary contribution. It is not clear a priori what value the boundary integral on the right hand side of Eq. (26) reaches when $\mathrm{Re}\to\infty$, so that a prediction of the time behavior of Ω in this limit is not straightforward. Although it is expected that in this limit the kinetic energy decay vanishes, it is not a priori guaranteed. In bounded no-slip domains, vorticity production at the boundaries might yield substantial growth of the enstrophy, and as a consequence the enstrophy need not be bounded by its initial value as in 2D unbounded and periodic domains.

4.1 Numerical Methods for 2D Turbulence in Confined Domains. The 2D turbulence computations in square, rectangular, and circular domains with no-slip boundaries reported in the literature are almost all based on spectral methods. We will briefly discuss the two main approaches, the Chebyshev pseudospectral method for simulations in square and rectangular domains and a spectral method based on Fourier–Bessel expansions for computations on a circular domain. Some unresolved issues associated with imposing no-slip boundary conditions at material walls for incompressible flows will conclude this section on numerical methods. A newly emerging approach, based on Fourier spectral methods with volume penalization, will briefly be introduced later on.

Numerical simulations of 2D turbulence in square (and rectangular) containers with no-slip walls are performed with a 2D Chebyshev pseudospectral method. Technical details of the numerical code are described elsewhere [133]. The flow domain $\mathcal{D}$ with boundary $\partial\mathcal{D}$ is a two-dimensional square cavity—in dimensionless form the square $[-1,1]\times[-1,1]$, Cartesian coordinates in a frame of reference are denoted by x and y, and the velocity field is denoted by $\mathbf{u}=(u,v)$. The equation governing the nondimensional (scalar) vorticity $\omega=\partial v/\partial x-\partial u/\partial y$ is obtained by taking the curl of the momentum equation. The following set of equations (describing the flow in the $(\omega,\mathbf{u})$-formulation) has to be solved numerically (for unforced flows):

$$\frac{\partial\omega}{\partial t} + (\mathbf{u}\cdot\nabla)\omega = \frac{1}{\mathrm{Re}}\nabla^2\omega \quad \text{in} \quad \mathcal{D} \tag{27}$$

$$\nabla^2\mathbf{u} = \hat{\mathbf{k}}\times\nabla\omega \quad \text{in} \quad \mathcal{D} \tag{28}$$

with the boundary condition $\mathbf{u}=0$ and enforcing $\hat{\mathbf{k}}\cdot\nabla\times\mathbf{u}=\omega$ on $\partial\mathcal{D}$ by an influence matrix technique. The details of this method can be found elsewhere [133]. The equivalence of Eqs. (27) and (28) and associated boundary conditions with the original formulation consisting of the vorticity equation (27), vorticity definition $\hat{\mathbf{k}}\cdot\nabla\times\mathbf{u}=\omega$ on the domain $\mathcal{D}$, incompressibility ($\nabla\cdot\mathbf{u}=0$) on $\mathcal{D}$, and $\mathbf{u}=0$ on $\partial\mathcal{D}$ has been shown by Daube [134]. An initial condition, $\omega|_{t=0}=\hat{\mathbf{k}}\cdot\nabla\times\mathbf{u}_0$, where $\mathbf{u}_0$ is the initial velocity field on $\mathcal{D}$, is also supplemented. The Reynolds number is defined as $\mathrm{Re}=UW/\nu$, with U as a characteristic velocity (based on the rms velocity of the initial flow field) and W as the half-width of the box. The time is made dimensionless with W/U, and $t\simeq 1$ is comparable with an initial eddy turnover time. Time discretization of the vorticity equation (27) is semi-implicit: It uses the explicit Adams–Bashforth scheme for the advection term and the implicit Crank–Nicolson procedure for the diffusive term.

The vorticity and both components of the velocity are expanded in a double truncated series of Chebyshev polynomials: The scalar vorticity and both components of the velocity field are $\omega(x,y,t)=\Sigma_{nm}\hat{\omega}_{nm}(t)T_n(x)T_m(y)$ and $\mathbf{u}(x,y,t)=\Sigma_{nm}\hat{\mathbf{u}}_{nm}(t)T_n(x)T_m(y)$, where the Chebyshev polynomials $T_n(x)=\cos(n\theta)$, with $\theta=\cos^{-1}(x)$ and a similar expression for $T_m(y)$. Here, $n\le N$ and $m\le N$; thus the number of active modes is $(N+1)^2$. An important advantage of using Chebyshev pseudospectral methods is the condensation of grid points near the boundaries; the distance between adjacent zeros near the boundaries is $\mathcal{O}(N^{-2})$. This property reflects one of the main advantages of using Chebyshev polynomials for flow simulations with no-slip boundaries, which require a high spatial resolution near the boundaries to resolve the steep vorticity gradients in the viscous boundary layers. Recently, benchmark computations of dipole-wall collisions have underlined the importance of this particular property of Chebyshev pseudospectral schemes [135]. Well-resolved boundary layers are directly relevant for 2D turbulence computations in bounded domains with no-slip walls.

Transformations from physical to spectral space, and vice versa, can be performed efficiently by employing fast Fourier transform (FFT) methods. All numerical calculations, except the evaluation of the nonlinear terms, are performed in spectral space; i.e., the coefficients $\hat{\mathbf{u}}_{nm}(t)$ and $\hat{\omega}_{nm}(t)$ are marched in time. FFT methods are used to evaluate the nonlinear terms following the procedure designed by Orszag [136], where the padding technique has been used for de-aliasing.

Numerical simulations of decaying 2D turbulence on a circular domain with a no-slip boundary are usually carried out with Chebyshev–Fourier pseudospectral codes (although the center of

the circular domain deserves special attention), thus enabling FFT methods for computation of the nonlinear term in the Navier–Stokes equations. The numerical studies by Li and Montgomery [129] and Li et al. [130,131] are based on a slightly different spectral method, viz., a Fourier–Bessel expansion. The starting point here are the Navier–Stokes equations in the $(\mathbf{u},p)$-formulation, together with incompressibility ($\boldsymbol{\nabla}\cdot\mathbf{u}=0$), and the Poisson equation for the stream function (related to the velocity field according to $\mathbf{u}=\boldsymbol{\nabla}\psi\times\hat{\mathbf{k}}$), $\boldsymbol{\nabla}^2\psi=-\omega$ in $\mathcal{D}$. Throughout, polar coordinates (r,θ) are used, and we choose $\psi=0$ and $\partial\psi/\partial r=0$ at the (no-slip) boundary of the circular domain ($r=a$). The stream function ψ is expanded in a set of orthogonal expansion functions $\psi_{mn}(r,\theta)$ believed to be a complete set for this problem (see the paper by Li et al. [131] for a more elaborate discussion),

$$\psi_{mn}(r,\theta)=C_{mn}\left(J_m(\gamma_{mn}r)-\frac{r^m}{a^m}J_m(\gamma_{mn}a)\right)e^{im\theta} \tag{29}$$

Here, $J_m(\gamma_{mn}r)$ is the ordinary Bessel function of the first kind, $m=0,1,2,\ldots$ and $n=1,2,\ldots$. Furthermore, C_{mn} is a constant to normalize $\mathbf{u}_{mn}=\boldsymbol{\nabla}\psi_{mn}\times\hat{\mathbf{k}}$ over the interior of the circle. The ψ_{mn} are defined for negative m by replacing $e^{im\theta}$ by $e^{-im\theta}$. From Eq. (29) it can be concluded that all $\psi_{mn}(r=a)=0$, thus vanishing the normal velocity component at the boundary. The coefficients γ_{mn} are chosen to satisfy the second boundary condition at $r=a$; thus there is no tangential velocity component at the boundary. The ψ_{mn} thus satisfy individually both boundary conditions.

The computational procedure starts with expanding the velocity field by $\mathbf{u}=\Sigma_{mn}\hat{\chi}_{mn}(t)\mathbf{u}_{mn}$ and substituting this expression in the Navier–Stokes equations. After taking the inner products with the individual $\mathbf{u}_{mn}$, an infinite set of coupled ordinary differential equations (ODEs) is obtained for the $\hat{\chi}_{mn}$. The pressure terms drop out in computing the inner products, which is due to the absence of a normal flow component at the material wall. The remaining system of ODEs is truncated in the manner of a Galerkin approximation, disregarding all the expansion coefficients and equations with $|m|>M$ and $n>N$. The computation takes place entirely in spectral space. The nonlinear terms in the ODEs (resulting from $(\mathbf{u}\cdot\boldsymbol{\nabla})\mathbf{u}$) appear as quadratic convolution sums with coupling coefficients that are definite integrals of three Bessel functions. These integrals have to be evaluated numerically with high accuracy and stored as a table (note that no analogon of 2D FFTs and padding techniques exists for the Fourier–Bessel system). The solution is advanced in time by employing adaptive step size fourth- and fifth-order Runge–Kutta methods.

The advantage of using a Fourier–Bessel spectral method is the implicit satisfaction of the boundary conditions and the fact that the method is unaffected by unphysical singularities in $r=0$ and that it does not suffer from aliasing errors. Chebyshev polynomials as used in Fourier–Chebyshev or 2D Chebyshev methods do not individually satisfy the boundary conditions, which have to be enforced by an additional set of equations. The disadvantage of employing Fourier–Bessel expansions is the lack of efficient transform and convolution algorithms. The computations have to be carried out in spectral space and have inherently a lower spatial resolution as the computations with a Fourier–Chebsyhev spectral method. The maximum Reynolds number that can be achieved is thus substantially smaller.

A final remark concerns unresolved ambiguities with the pressure determination that might be addressed mathematically in the future and is relevant for flows in domains with no-slip boundaries. This issue has recently been put forward by Kress and Montgomery [137]. Taking the divergence of the momentum equations leaves a Poisson equation for the pressure to be solved. For periodic boundary conditions, the pressure can be determined unambiguously. In the presence of rigid no-slip walls, however, both Dirichlet and Neumann boundary conditions on the pressure can be inferred from the Navier–Stokes equations and thus amount to an overdetermination. One cannot escape by employing the (ω,ψ)-formulation; the equation $\boldsymbol{\nabla}^2\psi=-\omega$ suffers from a similar overdetermination related to the boundary conditions for ψ. How it might affect the results obtained for turbulence simulations in, for example, square domains (based on the 2D Chebyshev pseudospectral algorithm) is yet unclear. The results discussed by Kress and Montgomery [137] might indicate that the effects are possibly of little consequence, but the issue needs to be resolved.

4.2 Quasi-2D Turbulence in Stratified Fluids: Laboratory Experiments. In this section we will review several remarkable properties of turbulent flows in square, rectangular, and circular containers with no-slip boundaries. We will in particular describe some experiments concerning quasi-2D decaying turbulence in linearly or in two-layer stratified fluids [126,128,138]. The quasi-2D flow in these experiments interacts at some stage with the no-slip domain boundaries. The decay scenario and the quasistationary final states in containers with rigid walls are the central topic, and we discuss the results in the framework of a few theoretical predictions introduced in Secs. 2.2 and 2.3.

The experiments on quasi-2D decaying turbulence were carried out in a circular container with radius $R=46$ cm and depth of 30 cm, a square container with dimensions of $100\times100\times30$ cm^3 (length $\times$ width $\times$ depth), and a rectangular container of typical dimensions of $200\times40\times30$ cm^3. For the latter case, the horizontal dimensions of the actual working flow domain were determined by the position of a removable wall mounted between the two longer sides of the container. In this way the aspect ratio δ, defined as the ratio between length and width of the working flow domain, could be varied. The containers were either filled with a two-layer salt stratification, consisting of a layer of fresh water on top of a layer of salty water, separated by an interfacial layer of typically a few centimeters depth or with a linearly stratified fluid. Typical buoyancy frequencies in these experiments were $N\approx2$ rad s^{-1}. Motion was generated by dragging a grid consisting of a linear array of vertical rods (3 mm diameter) horizontally through the fluid with a constant speed V. After having moved from one side to the opposite side of the tank, the grid was lifted out of the water (a detailed description of the forcing mechanism and flow visualization can be found elsewhere [126]). At large enough towing speed ($V\simeq15$ cm/s), the motion in the wake of the grid is turbulent. Similar experiments were performed by Yap and van Atta [139] and Fincham et al. [140], but in these experiments rigid boundaries are situated relatively far away and do not affect the stratified turbulence significantly.

Although strictly not 2D, the fluid motion shows the phenomenological characteristics of 2D turbulence, namely, the emergence of larger coherent vortex structures. This motion is very persistent, the decay mainly governed by vertical diffusion. A discussion of the dissipation of kinetic energy by vertical shearing (or vertical diffusion) in these experiments is given by Maassen et al. [126], and the dissipation of kinetic energy agrees with previous observations obtained in experiments of freely decaying stratified grid turbulence [140]. In particular, it was found that horizontal dissipation accounts for less than 20% of the total energy dissipation.

Two sets of experiments in circular containers have been reported [126,138]. In the first set the initial turbulent flow field does not contain any net angular momentum, $L_0\approx0$. The arrangement of the rods in the grid used for the second set of experiments is such that the initial flow field contains a substantial amount of angular momentum, $L_0\neq0$. The Reynolds number of the flow, defined as $\mathrm{Re}=UR/\nu$, with U as the rms velocity of the horizontal flow and R as the radius of the container, is approximately 4000. The experiments with $L_0\approx0$ show that the small vortices, which are formed in the wake of the rods, evolve according to the usual behavior of 2D turbulence: like-sign vortices merge, oppositely signed vortices form dipoles, and all vortices grow in size. Stream function contour plots of a typical run are displayed in Fig. 10.

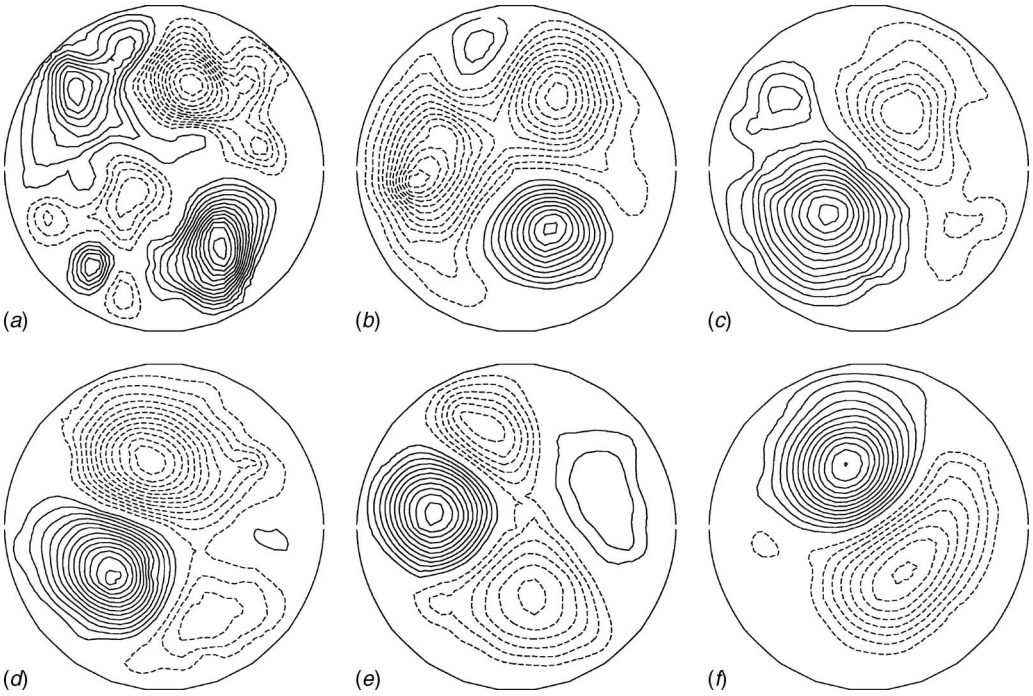

Fig. 10 Stream function contour plots of an experiment with $L_0 \approx 0$ in a circular container. Dashed contours represent negative stream function values, and solid contours represent positive values. The contour level increments are (*a*) 0.02, (*b*)–(*d*) 0.01, (*e*) 0.008, and (*f*) 0.004. Courtesy of Maassen et al. [126].

After a certain time, two strong vortices emerge, forming a dipolarlike structure that moves to the boundary of the container and pushes against the rigid wall (see Figs. 10(*c*) and 10(*f*)). Owing to the no-slip boundary condition, thin boundary layers are formed, in which the shear flow has oppositely signed vorticity. Subsequently, these filamentary vorticity patches are advected away from the boundary, into the interior. As a result, two new vortices are gradually formed behind the large dipole. Together with the primary dipole, these new vortices form an asymmetric quadrupolar structure (see Figs. 10(*d*) and 10(*e*)). The secondary dipole grows in size and finally fills the entire domain, whereafter the process described above is repeated several times until the newly formed dipole becomes sufficiently weak and nonlinearities become depleted.

All experiments in which the forcing rods were arranged in the grid such that they induced a modest net angular momentum $|L_0/L_{sb}| \approx 0.2$, with L_{sb} as the angular momentum of the same amount of fluid with the same kinetic energy in solid body rotation, revealed another decay scenario. The initial flow field contains a net large-scale rotation superimposed on the small-scale vortices. The large-scale rotation dominates the flow evolution, and finally one large monopolar vortex fills the domain completely.

The decay process described above agrees remarkably well with the numerical experiments by Li and Montgomery [129] and Li et al. [131]. Although the Reynolds numbers in these simulations are somewhat smaller than in the experiments, they clearly observed both scenarios described above for different initial net angular momenta. A comparison of late-time vorticity contour plots from a typical experiment and a numerical simulation show striking similarities, and are shown in Fig. 11. The initial horizontal integral-scale Reynolds number in the experiment and the simulation were similar, $\mathrm{Re} = \mathcal{O}(1000)$. Additionally, Li and Montgomery [129] and Li et al. [131] performed simulations with stress-free boundary conditions and initialized the flow as in the no-slip case with $L_0 = 0$. The final state found here is a quasistationary dipole filling the circular domain perfectly. No quadrupolarlike structures are formed due to the absence of boundary layers. Although comparisons with the predictions of quasistationary equilibrium states for bounded flows are instructive, they are not

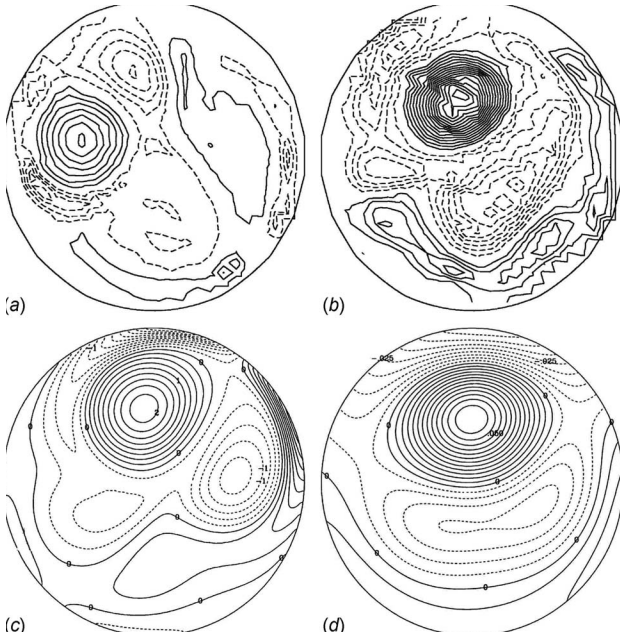

Fig. 11 (*a*) and (*b*) Vorticity contour plots of the late-time states emerging in the experiment shown in Fig. 10 (circular container, $L_0 \approx 0$) [126]. (*c*) and (*d*) Vorticity contour plots of the late-time states emerging in numerical simulations of decaying 2D turbulence on a circular domain with no-slip boundaries ($L_0 \approx 0$) [131]. For all panels: dashed contours represent negative values of vorticity, and solid contours represent positive values. Courtesy of Maassen et al. [126] and Li et al. [131].

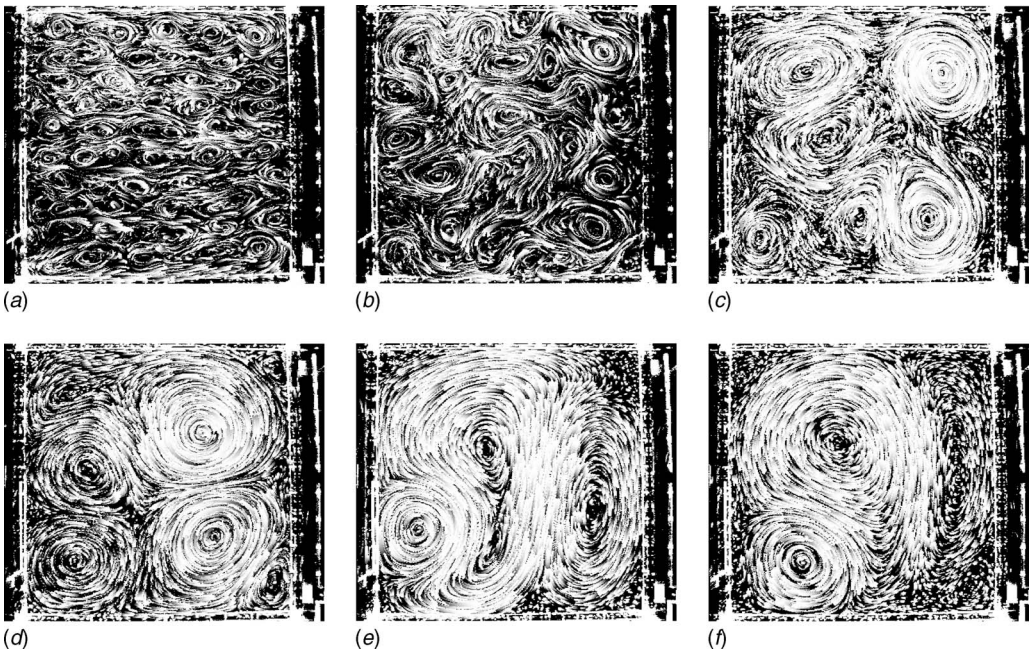

Fig. 12 Streak images of an experiment with $L_0 \approx 0$ in a square container. The tails of the streaks represent the displacements of tracer particles during an intervals of (*a*) and (*b*) 0.1, (*c*) and (*d*) 0.2, and (*e*) and (*f*) 4 dimensionless time units. Courtesy of Maassen et al. [126].

fully justified because these theories are formally developed for flows in domains with impermeable free-slip boundaries. The final state of the stress-free computation seems nevertheless consistent with the predictions by Pointin and Lundgren [88] and Chavanis and Sommeria [93], and a reasonable functional relation between ω and ψ can be extracted from the scatter plot, thus indicating $J(\omega,\psi)=0$. The simulations with no-slip boundary conditions and the experiments reveal a mixed picture. The predominantly quadrupolar late-time state for the case with $L_0=0$ does not agree with the predictions (see Fig. 4(*b*)). This is not completely surprising—flow-wall interactions are essential when the walls are no-slip—but underlines the difficulty to compare final states from laboratory experiments with equilibrium states from statistical-mechanical theories. Rather surprisingly, the experiments and simulations with initially a substantial amount of angular momentum reveal final states that agree with earlier predictions [88,93].

The quadrupolar final state observed above for decaying 2D turbulence with $L_0 \approx 0$ implies the absence of spontaneous spin-up for flows in circular containers. This is confirmed by measurements of $L(t)$ [126,138] and indicates that spontaneous spin-up is basically a result of the torque induced by pressure forces on the domain boundary. This contribution is absent in a circular domain, and torque generated by viscous shear is weak. The absence of spontaneous spin-up has been confirmed by Schneider and Farge [141]. Their simulations of decaying 2D turbulence at initial Reynolds number 5×10^4 show alternating periods of positive and negative angular momenta. On the other hand, the experiments revealed that initially nonzero angular momentum is persistent. It decays more slowly than the kinetic energy of the flow. Li et al. [130] numerically investigated the inverse cascade of angular momentum, if initially present, in such flows. It turns out that the angular momentum is an even more slowly decaying ideal invariant than the kinetic energy. It governs the decay scenario, as becomes clear from simulations and experiments, and it should be taken into account in theories predicting the most probable states. Analysis by Li et al. [130] shows that angular momentum cascades to lower azimuthal mode numbers and the angular momentum modal spectrum is eventually dominated by the lowest modes available. No indications of an inverse cascade have been observed if initially no angular momentum was present.

The laboratory experiments in square containers have been carried out in a similar way as those in circular containers. The initial Reynolds numbers are similar. A typical set of streak images from Maassen et al. [126] is displayed in Fig. 12. The initial stage of the decay process is basically the same as described earlier, but as the vortex structures become larger one of them starts to dominate the further evolution. The dominant vortex grows further in size by capturing like-sign vorticity or due to slow viscous growth until its size becomes comparable to the container dimension. Due to interaction with the no-slip boundaries, oppositely signed vorticity is generated near the boundaries that form smaller vortices. Numerical simulations show that the late-time decay is in nearly all cases characterized by the presence of a slowly rotating tripolar structure: a central slightly ellipsoidal vortex and two satellite vortices in which most of the boundary-layer vorticity is accumulated [79,111]. This state slowly relaxes toward a shielded monopole. These decay scenarios are characterized by spontaneous spin-up, irrespective of the presence or absence of initial angular momentum (see Fig. 9). It is the shielded monopole that is most frequently observed in the laboratory experiments due to the somewhat smaller initial Reynolds numbers compared with the simulations. Some of the late-time states are characterized by a strongly asymmetric dipolar structure with one dominating vortex and a smaller partner. These are characterized by weak spin-up of the flow. Asymmetric dipoles are hardly observed as late-time states in high-Reynolds number simulations.

The laboratory experiments performed in containers with different aspect ratios δ show the self-organization of an initially disordered quasi-2D flow toward a regular quasisteady cell pattern that fills the whole domain [128]. The number of vortices in these final cell patterns, N_f, depends on the aspect ratio of the flow domain, although its exact value cannot be predicted from the initial conditions. In most cases $N_f=\delta$ or $N_f=\delta\pm1$ was found. In some of the experiments, the initial flow field contains some net angular momentum. It appears that this bias has a large influence on the flow evolution in containers with $\delta=2$ or 3 but hardly influences the flow evolution for $\delta\geq4$. The most remarkable case is $\delta=2$. Here, the number of cells in the final state tends to be 2,

but examples of one or three cells are also found. Similar results are found for numerical simulations, provided that the Reynolds number is not too high; here Re=1000. Increasing the Reynolds number to 3000 in the simulations yields for nearly all runs one vortex as the final state (in a container with $\delta=2$). Experiments with an initial flow field containing angular momentum predominantly yield a three-vortex final state. Also the experiments with $\delta=3$ reveal a slightly larger number of vortices in the final state when initially angular momentum is added, viz., four versus three for the case with $L_0=0$.

Since the quasistationary states emerging in the experiments discussed above usually fill the whole domain, the shape of these structures depends on the geometry of the container. Solutions of the various statistical-mechanical theories, based on either point vortices or vortex patches, have been investigated systematically for the case of a bounded domain. The application of point vortices has been reported in several studies [88,89] where the maximum-entropy solutions of the sinh-Poisson equation on various bounded domains have been calculated. The use of the patch discretization to 2D flows in bounded domains has been addressed by Chavanis and Sommeria [93].

The late-time flow evolution in the experiments of decaying quasi-2D turbulence in stratified fluids [126] is in several cases similar to those reported earlier [109] for decaying turbulence in shallow fluid layers. A striking example is the formation of asymmetric dipoles, which led to the conclusion by Marteau et al. [109] that the final states in square domains disagree with statistical theories. Due to bottom friction, any nonlinearity is depleted in the shallow fluid-layer experiments, and further evolution toward a domain-sized vortex might be inhibited here in contrast with the experiments in stratified fluids. However, it remains difficult to infer from the experiments in square containers whether the statistical-mechanical approaches predict the right final states. For this purpose, it might be better to consider the decay scenarios for flows in rectangular containers [128]. The formation of a cell pattern of counter-rotating vortices was also predicted by maximum-entropy solutions for inviscid 2D flow on a bounded rectangular domain with $\delta\neq 1$. Pointin and Lundgren [88] computed the statistical equilibrium state of a system of positive and negative point vortices on a bounded rectangular domain, and for $\delta=2$ they predicted two cells of opposite circulations. Chavanis and Sommeria [93] predicted a dipolar solution, provided that $1.12<\delta\leq 2.0$ and $\Gamma=0$, and a single vortex for $|\Gamma|>\Gamma_{\mathrm{crit}}$ (see Sec. 2.3 and Fig. 4(*a*)). The laboratory experiments with $|L_0|>0$ preferably yield a three-vortex state. Caution is needed when comparing the two situations because in the experiment we still have $\Gamma=0$ due to the no-slip boundary condition. However, one strong central vortex (due to $|L_0|\neq 0$) in a $\delta=2$ container with rigid no-slip walls will inevitably produce two additional vortices with oppositely signed vorticities, originating from detached boundary layers, one in each end of the container. A three-vortex state will thus emerge. It is expected that the one-vortex prediction by Chavanis and Sommeria [93] for $|\Gamma|>\Gamma_{\mathrm{crit}}$ in a container with rigid no-slip walls will thus also yield a three-vortex state.

Since these maximum-entropy solutions do not take into account the effects of viscous boundary layers, the structure of these cell patterns [88,93] is thus entirely due to the rectangular geometry of the domain. Different decay scenarios for flows with no-slip and stress-free boundaries [128] indicate that the formation of cell patterns in laboratory experiments and in numerical simulations of decaying 2D turbulence is not merely determined by the shape of the container but also depends significantly on the formation and detachment of viscous boundary layers. This observation is further supported by the lack of correspondence with maximum-entropy solutions for a bounded domain with $\delta=2$, as presented in several studies [87,88,93]. Such a clear disagreement between predictions from statistical-mechanical theories and numerical simulations and experiments was not found for the square container case. However, the general case with circular or rectangular domains underlines the need for modified approaches to predict quasistationary final states in bounded domains.

4.3 Small-Scale Vorticity Production at No-Slip Boundaries. To estimate the vorticity production at the no-slip boundaries, a series of numerical experiments of a dipole collision with a no-slip wall has been conducted. The flow induced by the traveling dipole and the subsequent dipole-wall collision is not turbulent but contains the essential ingredients needed to estimate the enstrophy production at the walls. A well-defined initial condition of the flow has been chosen, i.e., a condition satisfying zero velocity and vorticity at the domain boundaries at $t=0$. In order to satisfy these constraints, a dipolar vortex structure, consisting of two equally strong, oppositely signed, isolated monopoles, is released in the center of the container and is allowed to collide with the boundary. This setup enables a systematic study of the Reynolds number dependence of the vorticity production, and a number of normal and oblique dipole-wall collisions have been investigated numerically. High vorticity values at the boundary are found during the collision, and the vorticity flux $(\partial\omega/\partial n)$ becomes extremely large after the impact of the dipole at the no-slip wall. Many thin vorticity filaments and small-scale vortices are produced.

A series of Reynolds numbers has been considered (up to Re $=1.6\times 10^5$) to reveal the scaling of the enstrophy with the Reynolds number. It can be shown, using $\omega_{\mathrm{bl}}/\delta_{\mathrm{bl}}\simeq\partial\omega/\partial n\propto\mathrm{Re}$, that the vorticity ω_{bl} contained by the thin boundary layers with thickness $\delta_{\mathrm{bl}}\propto 1/\sqrt{\mathrm{Re}}$ (from the flat-plate boundary-layer theory) scales as $\omega_{\mathrm{bl}}\propto\sqrt{\mathrm{Re}}$; thus $\Omega\propto\omega_{\mathrm{bl}}^2\delta_{\mathrm{bl}}\propto\sqrt{\mathrm{Re}}$. This scaling relation has been confirmed numerically [142]. As a consequence, the dissipation of kinetic energy (see Eq. (25)) scales with $1/\sqrt{\mathrm{Re}}$ instead of 1/Re. This indicates that the energy dissipation rate vanishes in the limit $\nu\rightarrow 0$, although at a much slower rate than for unbounded 2D flows.

The production of small-scale vorticity near no-slip walls is also reflected in 1D kinetic energy spectra measured close to the walls in numerical simulations [143] with $\mathrm{Re}=2\times 10^4$. Although we are not dealing with a conventional energy spectrum and the fact that the assumption of homogeneity and isotropy is most likely invalid near no-slip walls (which has yet to be proved), it is preferred to interpret the data in the Kolmogorov vocabulary of homogeneous isotropic turbulence. This vocabulary is thus strictly considered not applicable, but it enables straightforward comparison with previous studies. The spectra from Clercx and van Heijst [143] revealed a $k^{-5/3}$ inertial range during the initial decay stage, instead of a k^{-3} direct enstrophy cascade, due to the production of small-scale vorticity near no-slip boundaries. The direct enstrophy cascade is virtually absent at early times during the decay process. Similar runs with periodic boundary conditions were characterized by a direct enstrophy cascade with scaling close to k^{-3}. As an illustration we have plotted in Fig. 13 the averaged 1D energy spectra for a few runs with freely evolving 2D turbulence with $\mathrm{Re}=2\times 10^4$. The spectrum shown in Fig. 13(*a*) was computed after approximately four initial eddy turnover times. At later times the energy spectrum shows the buildup of a direct enstrophy cascade with a k^{-3} inertial range together with the inverse energy cascade for smaller wave numbers. The energy spectrum shows a kink, which slowly shifts to smaller wave numbers as time proceeds (see Fig. 13(*b*)). The position of the kink can clearly be associated with the growth of an averaged local boundary-layer thickness δ_{av}, with

$$\delta_{\mathrm{av}}\propto\sqrt{\oint_{\partial\mathcal{D}}\omega^2 ds/\oint_{\partial\mathcal{D}}\left(\frac{\partial\omega}{\partial n}\right)^2 ds} \tag{30}$$

It is expected that δ_{av} grows in the course of time. The strong correlation between the position of the kink in the spectrum and the average boundary-layer thickness is obvious from the data shown in Fig. 13(*c*) (for clarity we did not plot the data on top of

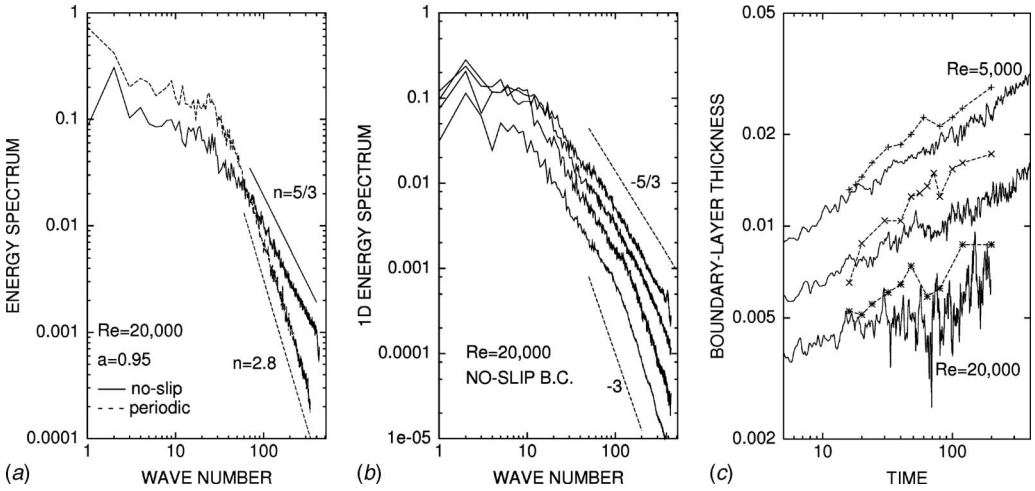

Fig. 13 (*a*) **The ensemble-averaged 1D energy spectra for runs with no-slip walls and with periodic boundary conditions (the steeper spectrum in the inertial range). (*b*) The time evolution of 1D spectra for runs with no-slip walls and (*c*) the growth of the average boundary-layer thickness δ_{av} (drawn spiky lines) compared with the position of the kink between $k^{-5/3}$ and k^{-3} behaviors. The symbols denote the position of the kink in the spectra (−−+−− for Re=5000, −−×−− for Re=10^4, and −−∗−− for Re=2×10^4). Taken from Clercx and van Heijst [143].**

each other; the spiky curves represent actually $\frac{1}{2}\delta_{av}$). New observations from laboratory experiments and numerical simulations of continuously forced quasi-2D turbulence have revealed similar spectra [124].

It is assumed that the $k^{-5/3}$ range represents an inverse energy cascade, but no evidence has been provided yet in the form of measurement of the fluxes that are not easily available for these flow configurations. Most likely, the approach introduced by Chen et al. [29,40] might provide ways to analyze the local transfer of energy and enstrophy, also near solid boundaries.

The production of high-amplitude vorticity in the boundary layers and the subsequent formation of many small and strong vortices will undoubtedly modify the vortex statistics. This is supported by numerical studies of decaying 2D Navier–Stokes turbulence in bounded domains with no-slip walls [78] that show an evolution of vortex statistics that is distinctly different from that predicted on the basis of the theory proposed by Carnevale et al. [67,68]. Moreover, a comparison with results from simulations where similar initial conditions have been used, but now with periodic boundary conditions, clearly indicates the importance of the no-slip walls as sources of small-scale vortices. In particular, the vortex density $\rho(t)$ shows a distinctly different power-law decay: $\rho_{ns}(t) \propto t^{-0.75}$ and $\rho_{per}(t) \propto t^{-1.03}$ for the runs with no-slip (ns) and periodic (per) boundary conditions, respectively (Re=10^4 in these runs). Additionally, the mean vortex separation increases significantly less in the decaying turbulence runs with no-slip boundaries compared with the runs with periodic boundary conditions, and the vorticity extremum of the strongest (and longest surviving) vortices decays substantially in the course of time (even if normalized by $\sqrt{E}$). In our view these data strongly suggest that application of the scaling theory [67,68] to decaying 2D Navier–Stokes turbulence in bounded domains with no-slip walls might be questionable. For fairness we should mention that it was never claimed by Carnevale et al. [67,68] that their theory might be valid for the evolution of the vortex population in bounded decaying 2D turbulence simulations with no-slip walls. However, many validation attempts of the scaling theory were based on laboratory experiments conducted in square or rectangular containers [70,71]. We believe that any agreement between experimentally obtained power-law exponents and the Carnevale approach is accidental. The experimental vortex statistics data also agree with the late-time viscosity-dominated decay stage of numerical simulations with no-slip boundaries [78,95,111,126].

4.4 Spin-Up in Decaying and Forced 2D Turbulence in Square Domains. Decaying 2D turbulence simulations in square domains with no-slip boundaries were first reported at the end of the 1990s. Two kinds of numerical experiments have been conducted: a set of numerical simulations with a random initial velocity field and relatively small integral-scale Reynolds numbers ($1000 \le \mathrm{Re} \le 2000$) [111,127] and another set with 10×10 slightly perturbed Gaussian vortices on a rectangular lattice. The integral-scale Reynolds number for this latter set of simulations is considerably higher [78,79]: $5000 \le \mathrm{Re} \le 20{,}000$. Probably the most surprising observation from these simulations is the spontaneous formation of large-scale mean rotation, with equal probability of either clockwise or anticlockwise rotation, starting with an initial flow field that contains zero net angular momentum. Currently, with the development of advanced algorithms based on volume penalization [144,145] combined with parallelized Fourier pseudospectral codes, it has been possible to mimic the presence of no-slip walls [146]. With this approach the decaying 2D turbulence simulations become competitive with classical 2D turbulence simulations with periodic boundary conditions. Decaying 2D turbulence simulations in confined domains with resolutions up to 4096^2 Fourier modes have been carried out (and initial integral-scale Reynolds numbers up to 2×10^5). These studies revealed that spontaneous spin-up is a persistent phenomenon not particularly related to low or medium Reynolds number flows [147].

The flow evolution of decaying 2D turbulence on a square domain with no-slip walls and initial integral-scale Reynolds number Re=10^5 is characterized by a rapid self-organization due to merging of like-sign vortices and the formation of dipoles. Strong vortex-wall interactions occur, and the formation of increasingly larger coherent structures is observed. In particular, the simulations by Keetels et al. [147] reveal the emergence of many very small vortices with high vorticity amplitude, which can directly be traced back toward thin vorticity filaments released from the no-slip walls (see Fig. 14). The late-time stage seems to indicate a relaxation toward a quasistationary final state via a global large-scale circulation cell (see also Fig. 14(*d*)).

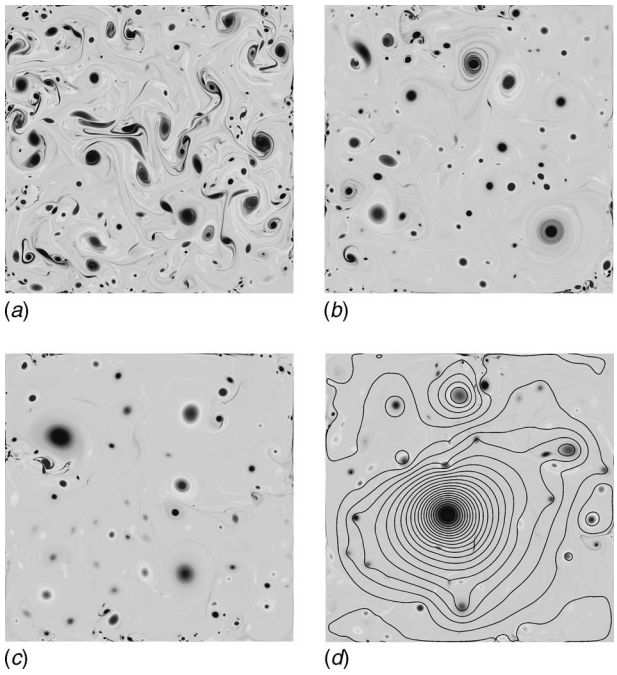

Fig. 14 Vorticity plots of simulation with an initial Reynolds numer $\mathrm{Re}=10^5$ and 4096^2 Fourier modes.

It was shown by Molenaar et al. [105] that spin-up-like phenomena may also be observed if a time-dependent forcing $Q(\mathbf{r},t)$ is applied to the vorticity equation, generating a 2D fluid flow from zero initial conditions, $\omega_0(\mathbf{r})=0$. The stochastic forcing protocol is a first-order Markov chain, introduced by Lilly [16] and described in some detail by Maltrud and Vallis [34]. In discrete-time notation, the first-order Markov chain with correlation coefficient s and amplitude A_0, applied to wavevector $\mathbf{k}$, reads as

$$Q(\mathbf{k},n) = sQ(\mathbf{k},n-1) + \sqrt{1-s^2}A_0 e^{i\pi\psi(\mathbf{k},n)} \tag{31}$$

where the random variable $\psi(\mathbf{k},n)$ is drawn from a Gaussian distribution. The Markov chain is applied to a shell of wave numbers $|\mathbf{k}| \in [7,9]$ with $A_0=6.0$ and $s=0.98$ (see Molenaar et al. [105] for details). The forcing scale is similar to that used by Sommeria [102] in his experiments in a shallow layer of mercury. The integral-scale Reynolds number is based on the time- and domain-averaged rms velocity, achieving a value on the order of 3000.

As in the case of decaying flow, for these stochastically forced flows the phenomenology is dominated by the generation of a large circulation cell, occupying most of the interior of the domain. However, in contrast to the decaying case, in the forced flow several consecutive events of rapid buildup and collapse of the circulation cell occur, where a spontaneous sign reversal of the angular momentum of the flow is possible from one event to the next. A typical example of the evolution of the normalized angular momentum $\tilde{L}(t)=L(t)/L_{\mathrm{sb}}(t)$, with $L_{\mathrm{sb}}(t)$ as in Sec. 4.2, is shown in Fig. 15. It is clearly seen that $\tilde{L}(t)$ tends to reach a nonzero value; i.e., the flow exhibits spontaneous spin-up. Moreover, several sign changes in $\tilde{L}$ are observed to occur a couple of times: apparently the flow reverses abruptly in those cases. Such a sequence of events is also shown in Fig. 16 in three consecutive snapshots of the vorticity field, depicting a breakdown and a subsequent buildup, with opposite signs, of a large coherent structure. These observations complement experimental results [102,116], although the bottom friction is relevant for these experiments. Due to the very limited experimental resolution, the mechanism explaining the large-scale reversals remained unclear. The present simulations clearly indicate that the reversals are initiated by

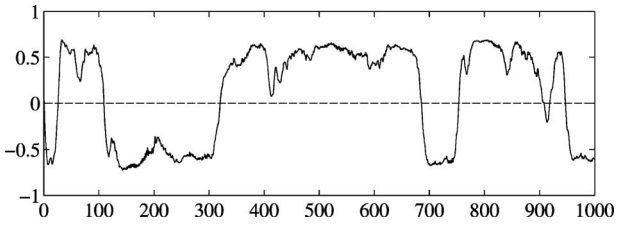

Fig. 15 Evolution of the normalized angular momentum $\tilde{L}(t)=L(t)/L_{\mathrm{sb}}(t)$, showing distinct phases of spin-up. For this run $\mathrm{Re}\simeq 3000$, $A_0=6.0$, and $\sigma=0.98$. This figure is taken from Molenaar et al. [105].

boundary-layer formation and its subsequent detachment and roll-up to form small strong vortices. These small vortices erode the central cell, which might eventually collapse.

Time series of the energy and enstrophy, normalized by their respective mean values, are shown in Fig. 17. The time series cover approximately 300 eddy turnover times. In the energy time series, the spin-up effect is clearly recognizable in the form of clear peaks, reaching up to three times average values. These peaks correspond to a condensation of energy within the large circulation cell, as was conjectured by Kraichnan [10]. The evolution of the enstrophy is directly influenced by the formation of viscous boundary layers at the no-slip walls. These boundary layers are sources of opposite-signed vorticity, as compared with the central cell. Hence, these structures are sources of enstrophy $\Omega(t)$, which is proportional to the destruction term in the global energy balance.

The global phenomenological picture is in sharp contrast with observations of forced 2D turbulence on a double-periodic domain. There the usual end state is a domain-filling dipole structure, as was first observed in DNS by Hossain et al. [20] and later by Smith and Yakhot [24]. Moreover, the present observations highlight another important difference with continuously forced flows in a double-periodic domain. For these periodic domains often some kind of additional energy dissipation is applied in order to achieve a statistically stationary energy balance. For the forced wall-bounded flows considered here, it is found that the no-slip walls provide a natural energy dissipation mechanism by means of the generation of viscous boundary layers.

A simple physical idea follows from the observation that the energy scales with velocity squared, $E(t)\propto|\mathbf{u}|^2$, and the absolute angular momentum scales with a finite length times velocity, $|L(t)|\propto r|\mathbf{u}|$. Hence, on dimensional grounds, one has $\gamma E(t)=|L(t)|$, which defines the time $\gamma=\frac{1}{2}|\int_{\mathcal{D}} r^2\omega(\mathbf{r},t)dA|/E(t)$. Here, $\gamma=\mathcal{O}(1)$ implies a strong similarity in the evolution of $E(t)$ and $|L(t)|$, which seems to coincide with a self-organization of the flow into a large vortex structure. This similarity regime indeed occurs in the computational data, as can be seen in the upper graph of Fig. 17. Assuming that γ is a constant, preferably of the order of unity $\gamma=\mathcal{O}(1)$, it can be shown that the approximate equality $E(t)\sim|L(t)|$ is only satisfied if $E(t)\leq C_0(\mathcal{D})\simeq 5.3$ and if $Z(t)\geq C_1(\mathcal{D})\simeq 26.3$. The proof of these bounds and the calculation of the numerical values for $C_0(\mathcal{D})$ and $C_1(\mathcal{D})$ can be found elsewhere [105]. Both bounds are seen to be crudely satisfied in Fig. 17, where $C_1(\mathcal{D})$ is indicated in the lower graph, whereas $C_0(\mathcal{D})$ lies outside the scale of the upper graph.

The present numerical results for decaying and forced 2D turbulence, which clearly show the phenomenon of spontaneous spin-up and, for the forced case, the sudden reversals of the large-scale circulation, clarify several of the open questions put forward by Sommeria [102] concerning the mean flow in the experiments. The interaction of the flow with the lateral no-slip sidewalls is essential for the buildup of angular momentum of the flow. Basically two contributions are relevant: torques due to pressure forces

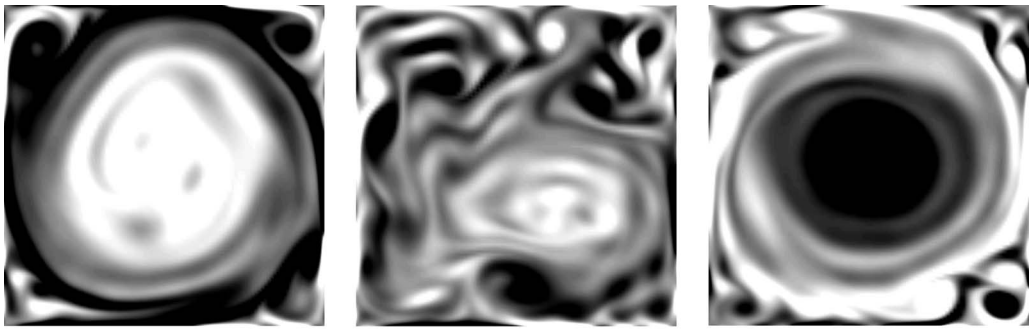

Fig. 16 Snapshots of the vorticity evolution during the sign reversal of a large monopolar vortex structure with vorticity levels ranging from $\omega<-5$ (black) to $\omega>5$ (white). Same run as shown in Fig. 15. This figure is taken from Molenaar et al. [105].

and due to viscous shear and normal stresses, with the former as a dominant contribution. Sommeria [102] already identified the role of the pressure forces at the domain boundary as an important source for angular momentum production. He did not address the role of the no-slip boundary condition, and neither did he notice any well-defined mechanism for the reversals although he did suspect that the large-scale recirculation cell is destabilized by small eddies. The numerical results clearly identify the no-slip boundaries, which act as strong sources of small-scale vorticity, as the cause of the reversals. An issue not yet resolved is the fact that his laboratory results show decreasing probability of reversals with decreasing bottom friction (no reversals were observed for $\mathrm{Re}_M > 41$; see Sec. 3.1). The forced 2D turbulence simulations (without Rayleigh friction) do show such reversals.

5 Outlook

Recent investigations of 2D Navier–Stokes turbulence in bounded domains heavily relied on the knowledge of 2D turbulence that has been built up during the past 40 years and on the well-designed laboratory experiments that enabled many investigators to probe quasi-2D turbulence in the laboratory. However, the type of boundary condition apparently plays an important role in the evolution of confined 2D turbulence, both for the decaying and the continuously forced case. It has been found in laboratory experiments as well as in numerical simulations of decaying 2D turbulence on domains with no-slip walls that the temporal evolution of the vortices and the quasistationary late-time state of the flow differ substantially from the classical predictions [67,68,81,88,93]. Laboratory experiments, with initial motion ($\mathrm{Re}\approx 5000$) generated by a translating grid, and high-resolution numerical simulations (with $\mathrm{Re}=2\times10^3-2\times10^5$) have revealed the crucial role of the no-slip walls, viz., as sources of high-amplitude vorticity filaments. These filamentary structures are advected away from the walls and hence affect the flow evolution in the interior. A remarkable feature in the evolution is the so-called spontaneous spin-up. At this stage the total angular momentum L shows a rapid increase (even when starting with an initial state with $L_0\approx 0$), thus revealing the role of the walls in providing forces (both normal and shear stresses) and torques that lead to a change in L.

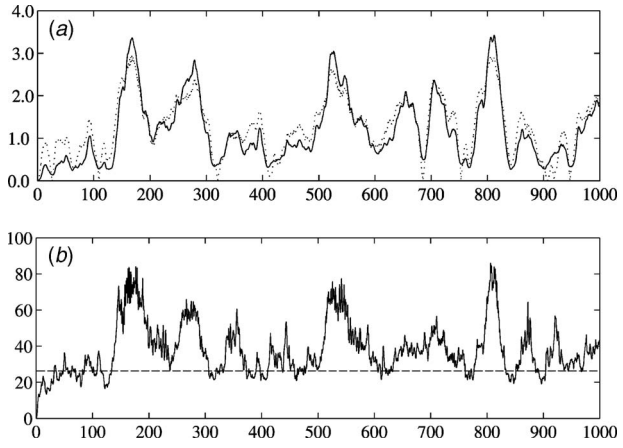

Fig. 17 Similarity in the behavior of the kinetic energy (solid line) and the absolute angular momentum (dotted) in the upper graph. The lower graph shows the enstrophy (solid line) and the lower bound (dashed). These figures are taken from Molenaar et al. [105].

The remarkable role of no-slip walls is also observed in high-resolution simulations of continuously forced turbulence. In confined forced flows, the motion becomes organized in a single large cell and is characterized by a repeated process of cell buildup and destruction. This is in marked contrast to the flow behavior observed in forced 2D turbulence on a double-periodic domain [20,24]. Open questions here are as follows: What determines the dynamics of the reversals? Are these characterized by low-dimensional dynamics or has it a purely stochastic origin? Because of the role of the no-slip walls as sources of high-amplitude vorticity filaments, the presence of no-slip boundaries might also modify the scaling behavior of certain structure functions (such as for vorticity increments) and possibly induce small-scale intermittency. No-slip boundaries as a source of small-scale high-amplitude vorticity, thus as a source of enstrophy and palinstrophy [78,142,143], will modify the dissipation of energy and enstrophy. However, these issues are hardly quantified, and mathematical tools similar to those employed for unbounded 2D turbulence [5,41,43,65] might prove very useful to provide estimates and bounds on vorticity production at no-slip walls, energy and enstrophy dissipation, angular momentum, etc.

The observations reveal that the presence of no-slip boundaries affects the behavior of 2D turbulence (either continuously forced or decaying) in a rather dramatic way, their influence not being restricted to regions close to the perimeter but essentially extending over the full domain. Any comparison of laboratory experiments or numerical simulations of 2D flows confined by no-slip walls with corresponding results for inviscid flow on doubly periodic domains requires caution.

Finally, it is expected that recent theoretical developments, such as the approach introduced by Chen et al. [29,40] and Eyink [50], will improve our understanding of local energy and enstrophy transfers in the neighborhood of rigid no-slip walls. Moreover, novel numerical algorithms, such as volume penalization [141,146,147], allowing the use of relatively cheap parallelized Fourier pseudospectral codes for 2D bounded turbulence simula-

tions, will advance studies on 2D Navier–Stokes turbulence in bounded domains substantially in the years to come.

Acknowledgment

The authors gratefully acknowledge financial support from the Dutch Foundation for Fundamental Research on Matter (FOM) (Program 36 "Two-Dimensional Turbulence"). This work was sponsored by the Stichting Nationale Computerfaciliteiten (National Computing Facilities Foundation (NCF)) for the use of supercomputer facilities, with financial support from the Netherlands Organization for Scientific Research (NWO).

References

[1] Kraichnan, R. H., and Montgomery, D., 1980, "Two-Dimensional Turbulence," Rep. Prog. Phys., **43**, pp. 547–619.
[2] Danilov, S. D., and Gurarie, D., 2000, "Quasi-Two-Dimensional Turbulence," Phys. Usp., **43**, pp. 863–900.
[3] Tabeling, P., 2002, "Two-Dimensional Turbulence: A Physicist Approach," Phys. Rep., **362**, pp. 1–62.
[4] Kellay, H., and Goldburg, W. I., 2002, "Two-Dimensional Turbulence: A Review of Some Recent Experiments," Rep. Prog. Phys., **65**, pp. 845–894.
[5] Doering, C. H., and Newton, P. K., 2007, "Introduction to Special Issue: Mathematical Fluid Dynamics," J. Math. Phys., **48**, p. 065101 (see also other contributions in this issue).
[6] Onsager, L., 1949, "Statistical Hydrodynamics," Nuovo Cimento, **6**, pp. 279–287.
[7] Fjørtoft, R., 1953, "On the Changes in the Spectral Distribution of Kinetic Energy for Two-Dimensional Non-Divergent Flow," Tellus, **5**, pp. 225–230.
[8] Lee, T. D., 1952, "On Some Statistical Properties of Hydrodynamical and Magneto-Hydrodynamical Fields," Q. Appl. Math., **10**, pp. 69–74.
[9] Similar statements can be made for ideal 3D turbulence and ideal 2D and 3D magnetohydrodynamic turbulence.
[10] Kraichnan, R. H., 1967, "Inertial Ranges in Two-Dimensional Turbulence," Phys. Fluids, **10**, pp. 1417–1423.
[11] Shebalin, J. V., 1989, "Broken Ergodicity and Coherent Structure in Homogeneous Turbulence," Physica D, **37**, pp. 173–191.
[12] Shebalin, J. V., 1998, "Phase Space Structure in Ideal Homogeneous Turbulence," Phys. Lett. A, **250**, pp. 319–322.
[13] Kraichnan, R. H., 1971, "Inertial-Range Transfer in Two and Three-Dimensional Turbulence," J. Fluid Mech., **47**, pp. 525–535.
[14] Leith, C. E., 1968, "Diffusion Approximation for Two-Dimensional Turbulence," Phys. Fluids, **11**, pp. 671–673.
[15] Batchelor, G. K., 1969, "Computation of the Energy Spectrum in Homogeneous Two-Dimensional Turbulence," Phys. Fluids, **12**, pp. II-233–II-239.
[16] Lilly, D., 1969, "Numerical Simulation of Two-Dimensional Turbulence," Phys. Fluids, **12**, pp. II-240–II-249.
[17] In this review we do not devote much space to the role of different forcing functions to drive 2D turbulence. The most obvious distinction is between random forcing in space and fixed steady-state forcing in some wave number band. These do not necessarily lead to the same flow configurations. This difference is particularly relevant for the question regarding what constitutes and what is to be expected from the forcing in real experimental configurations as can be found in the laboratory and in large-scale geophysical and planetary flows.
[18] Boffetta, G., 2007, "Energy and Enstrophy Fluxes in the Double Cascade of Two-Dimensional Turbulence," J. Fluid Mech., **589**, pp. 253–260.
[19] Fyfe, D., Montgomery, D., and Joyce, G., 1977, "Dissipative, Forced Turbulence in Two-Dimensional Magnetohydrodynamics," J. Plasma Phys., **17**, pp. 369–398.
[20] Hossain, M., Matthaeus, W. H., and Montgomery, D., 1983, "Long-Time States of Inverse Cascades in the Presence of a Maximum Length Scale," J. Plasma Phys., **30**, pp. 479–493.
[21] Frisch, U., and Sulem, P.-L., 1984, "Numerical Simulation of the Inverse Cascade in Two-Dimensional Turbulence," Phys. Fluids, **27**, pp. 1921–1923.
[22] Herring, J. R., and McWilliams, J. C., 1985, "Comparison of Direct Numerical Simulation of Two-Dimensional Turbulence With Two-Point Closure: The Effects of Intermittency," J. Fluid Mech., **153**, pp. 229–242.
[23] Siggia, E. D., and Aref, H., 1981, "Point-Vortex Simulation of the Inverse Energy Cascade in Two-Dimensional Turbulence," Phys. Fluids, **24**, pp. 171–173.
[24] Smith, L. M., and Yakhot, V., 1993, "Bose Condensation and Small-Scale Structure Generation in a Random Force Driven 2D Turbulence," Phys. Rev. Lett., **71**, pp. 352–355.
[25] Chertkov, M., Connaughton, C., Kolokolov, I., and Lebedev, V., 2007, "Dynamics of Energy Condensation in Two-Dimensional Turbulence," Phys. Rev. Lett., **99**, p. 084501.
[26] Borue, V., 1994, "Inverse Energy Cascade in Stationary Two-Dimensional Homogeneous Turbulence," Phys. Rev. Lett., **72**, pp. 1475–1478.
[27] Danilov, S., and Gurarie, D., 2001, "Nonuniversal Features of Forced Two-Dimensional Turbulence in the Energy Range," Phys. Rev. E, **63**, p. 020203.
[28] Boffetta, G., Celani, A., and Vergassola, M., 2000, "Inverse Energy Cascade in Two-Dimensional Turbulence: Deviations From Gaussian Behavior," Phys. Rev. E, **61**, pp. R29–R32.
[29] Chen, S., Ecke, R. E., Eyink, G. L., Rivera, M., Wan, M., and Xiao, Z., 2006, "Physical Mechanism of the Two-Dimensional Inverse Energy Cascade," Phys. Rev. Lett., **96**, p. 084502.
[30] Saffman, P. G., 1995, *Vortex Dynamics*, Cambridge University Press, Cambridge, UK.
[31] Moffatt, H. K., 1986, *Advances in Turbulence*, G. Comte-Bellot and J. Mathieu, eds., Springer, Berlin, p. 284.
[32] Legras, B., Santangelo, P., and Benzi, R., 1988, "High-Resolution Numerical Experiments for Forced Two-Dimensional Turbulence," Europhys. Lett., **5**, pp. 37–42.
[33] Ohkitani, K., 1991, "Wave Number Space Dynamics of Enstrophy Cascade in a Forced Two-Dimensional Turbulence," Phys. Fluids A, **3**, pp. 1598–1611.
[34] Maltrud, M. E., and Vallis, G. K., 1991, "Energy Spectra and Coherent Structures in Forced Two-Dimensional and Beta-Plane Turbulence," J. Fluid Mech., **228**, pp. 321–342.
[35] Borue, V., 1993, "Spectral Exponents of Enstrophy Cascade in Stationary Two-Dimensional Homogeneous Turbulence," Phys. Rev. Lett., **71**, pp. 3967–3970.
[36] Gotoh, T., 1998, "Energy Spectrum in the Inertial and Dissipation Ranges of Two-Dimensional Steady Turbulence," Phys. Rev. E, **57**, pp. 2984–2991.
[37] Lindborg, E., and Älvelius, K., 2000, "The Kinetic Energy Spectrum of the Two-Dimensional Enstrophy Turbulent Cascade," Phys. Fluids, **12**, pp. 945–947.
[38] Ishihara, T., and Kaneda, Y., 2001, "Energy Spectrum in the Enstrophy Transfer Range of Two-Dimensional Forced Turbulence," Phys. Fluids, **13**, pp. 544–547.
[39] Pasquero, C., and Falkovich, G., 2002, "Stationary Spectrum of Vorticity Cascade in Two-Dimensional Turbulence," Phys. Rev. E, **65**, p. 056305.
[40] Chen, S., Ecke, R. E., Eyink, G. L., Wang, X., and Xiao, Z., 2003, "Physical Mechanism of the Two-Dimensional Enstrophy Cascade," Phys. Rev. Lett., **91**, p. 214501.
[41] Tran, C. V., and Shepherd, T. G., 2002, "Constraints on the Spectral Distribution of Energy and Enstrophy Dissipation in Forced Two-Dimensional Turbulence," Physica D, **165**, pp. 199–212.
[42] Tran, C. V., and Bowman, J. C., 2003, "On the Dual Cascade in Two-Dimensional Turbulence," Physica D, **176**, pp. 242–255.
[43] Alexakis, A., and Doering, C. R., 2006, "Energy and Enstrophy Dissipation in Steady State 2D Turbulence," Phys. Lett. A, **359**, pp. 652–657.
[44] Eyink, G. L., 1996, "Exact Results on Stationary Turbulence in 2D: Consequences of Vorticity Conservation," Physica D, **91**, pp. 97–142.
[45] Dubos, T., and Babiano, A., 2002, "Two-Dimensional Cascades and Mixing: A Physical Space Approach," J. Fluid Mech., **467**, pp. 81–100.
[46] Babiano, A., and Provenzale, A., 2007, "Coherent Vortices and Tracer Cascades in Two-Dimensional Turbulence," J. Fluid Mech., **574**, pp. 429–448.
[47] Rivera, M. K., Daniel, W. B., Chen, S. Y., and Ecke, R. E., 2003, "Energy and Enstrophy Transfer in Decaying Two-Dimensional Turbulence," Phys. Rev. Lett., **90**, p. 104502.
[48] Kraichnan, R. H., 1975, "Statistical Dynamics of Two-Dimensional Flow," J. Fluid Mech., **67**, pp. 155–175.
[49] Eyink, G. L., 2006, "Multi-Scale Gradient Expansion of the Turbulent Stress Tensor," J. Fluid Mech., **549**, pp. 159–190.
[50] Eyink, G. L., 2006, "A Turbulent Constitutive Law for the Two-Dimensional Inverse Energy Cascade," J. Fluid Mech., **549**, pp. 191–214.
[51] Kraichnan, R. H., 1976, "Eddy Viscosity in Two and Three Dimensions," J. Atmos. Sci., **33**, pp. 1521–1536.
[52] Lilly, D. K., 1971, "Numerical Simulation of Developing and Decaying Two-Dimensional Turbulence," J. Fluid Mech., **45**, pp. 395–415.
[53] For bounded domains with no-slip walls, additional boundary contributions should be added to the right hand side of Eq. (14). In particular, the condition $\Omega(t) \leq \Omega(t=0)$ for flows in domains with no-slip boundaries is invalidated, as we will see later on in this review. Note that the equation describing the rate of change of kinetic energy remains unaffected by the presence of walls. However, the relation for $d\Omega/dt$ will change.
[54] Fornberg, B., 1977, "Numerical Study of 2-D Turbulence," J. Comput. Phys., **25**, pp. 1–31.
[55] Matthaeus, W. H., and Montgomery, D., 1980, "Selective Decay Hypothesis at High Mechanical and Magnetic Reynolds Numbers," Ann. N.Y. Acad. Sci., **357**, pp. 203–222.
[56] Basdevant, C., Legras, B., and Sadourny, R., 1981, "A Study of Barotropic Model Flows: Intermittency, Waves and Predictability," J. Atmos. Sci., **38**, pp. 2305–2326.
[57] McWilliams, J. C., 1984, "The Emergence of Isolated Coherent Vortices in Turbulent Flow," J. Fluid Mech., **146**, pp. 21–43.
[58] Santangelo, P., Benzi, R., and Legras, B., 1989, "The Generation of Vortices in High-Resolution, Two-Dimensional Decaying Turbulence and the Influence of Initial Conditions on the Breaking of Self-Similarity," Phys. Fluids A, **1**, pp. 1027–1034.
[59] Kida, S., 1985, "Numerical Simulation of Two-Dimensional Turbulence With High Symmetry," J. Phys. Soc. Jpn., **54**, pp. 2840–2854.
[60] Brachet, M. E., Meneguzzi, M., and Sulem, P.-L., 1986, "Small-Scale Dynamics of High-Reynolds Number Two-Dimensional Turbulence," Phys. Rev. Lett., **57**, pp. 683–686.
[61] Brachet, M. E., Meneguzzi, M., Politano, H., and Sulem, P.-L., 1988, "The Dynamics of Freely Decaying Two-Dimensional Turbulence," J. Fluid Mech., **194**, pp. 333–349.
[62] Benzi, R., Patarnello, S., and Santangelo, P., 1987, "On the Statistical Proper-

ties of Two-Dimensional Decaying Turbulence," Europhys. Lett., **3**, pp. 811–818.
[63] Benzi, R., Patarnello, S., and Santangelo, P., 1988, "Self-Similar Coherent Structures in Two-Dimensional Decaying Turbulence," J. Phys. A, **21**, pp. 1221–1237.
[64] McWilliams, J. C., 1990, "A Demonstration of the Suppression of Turbulent Cascades by Coherent Vortices in Two-Dimensional Turbulence," Phys. Fluids A, **2**, pp. 547–552.
[65] Tran, C. V., and Dritschel, D. G., 2006, "Vanishing Enstrophy Dissipation in Two-Dimensional Navier–Stokes Turbulence in the Inviscid Limit," J. Fluid Mech., **559**, pp. 107–116.
[66] Leith, C. E., 1984, "Minimum Enstrophy Vortices," Phys. Fluids, **27**, pp. 1388–1395.
[67] Carnevale, G. F., McWilliams, J. C., Pomeau, Y., Weiss, J. B., and Young, W. R., 1991, "Evolution of Vortex Statistics in Two-Dimensional Turbulence," Phys. Rev. Lett., **66**, pp. 2735–2737.
[68] Carnevale, G. F., McWilliams, J. C., Pomeau, Y., Weiss, J. B., and Young, W. R., 1992, "Rates, Pathways, and End States of Nonlinear Evolution in Decaying Two-Dimensional Turbulence: Scaling Theory Versus Selective Decay," Phys. Fluids A, **4**, pp. 1314–1316.
[69] Weiss, J. B., and McWilliams, J. C., 1993, "Temporal Scaling Behavior of Decaying Two-Dimensional Turbulence," Phys. Fluids A, **5**, pp. 608–621.
[70] Cardoso, O., Marteau, D., and Tabeling, P., 1994, "Quantitative Experimental Study of the Free Decay of Quasi-Two-Dimensional Turbulence," Phys. Rev. E, **49**, pp. 454–461.
[71] Hansen, A. E., Marteau, D., and Tabeling, P., 1998, "Two-Dimensional Turbulence and Dispersion in a Freely Decaying System," Phys. Rev. E, **58**, pp. 7261–7271.
[72] Bracco, A., McWilliams, J. C., Murante, G., Provenzale, A., and Weiss, J. B., 2000, "Revisiting Freely Decaying Two-Dimensional Turbulence at Millennial Resolution," Phys. Fluids, **12**, pp. 2931–2941.
[73] McWilliams, J. C., 1990, "The Vortices of Two-Dimensional Turbulence," J. Fluid Mech., **219**, pp. 361–385.
[74] Dritschel, D. G., 1993, "Vortex Properties of Two-Dimensional Turbulence," Phys. Fluids A, **5**, pp. 984–997.
[75] Chasnov, J. R., 1997, "On the Decay of Two-Dimensional Homogeneous Turbulence," Phys. Fluids, **9**, pp. 171–180.
[76] Dmitruk, P., and Montgomery, D. C., 2005, "Numerical Study of the Decay of Enstrophy in a Two-Dimensional Navier-Stokes Fluid in the Limit of Very Small Viscosities," Phys. Fluids, **17**, p. 035114.
[77] Bartello, P., and Warn, T., 1996, "Self-Similarity of Decaying Two-Dimensional Turbulence," J. Fluid Mech., **326**, pp. 357–372.
[78] Clercx, H. J. H., and Nielsen, A. H., 2000, "Vortex Statistics for Turbulence in a Container With Rigid Boundaries," Phys. Rev. Lett., **85**, pp. 752–755.
[79] Clercx, H. J. H., Nielsen, A. H., Torres, D. J., and Coutsias, E. A., 2001, "Two-Dimensional Turbulence in Square and Circular Domains With No-Slip Walls," Eur. J. Mech. B/Fluids, **20**, pp. 557–576.
[80] van Bokhoven, L. J. A., Trieling, R. R., Clercx, H. J. H., and van Heijst, G. J. F., 2007, "Influence of Initial Conditions on Decaying Two-Dimensional Turbulence," Phys. Fluids, **19**, p. 046601.
[81] Matthaeus, W. H., Stribling, W. T., Martinez, D., Oughton, S., and Montgomery, D., 1991, "Decaying, Two-Dimensional, Navier-Stokes Turbulence at Very Long Times," Physica D, **51**, pp. 531–538.
[82] Yin, Z., Montgomery, D. C., and Clercx, H. J. H., 2003, "Alternative Statistical-Mechanical Descriptions of Decaying Two-Dimensional Turbulence in Terms of 'Patches' and 'Points'," Phys. Fluids, **15**, pp. 1937–1953.
[83] Eyink, G. L., and Sreenivasan, K. R., 2006, "Onsager and the Theory of Hydrodynamic Turbulence," Rev. Mod. Phys., **78**, pp. 87–135.
[84] Matthaeus, W. H., Stribling, W. T., Martinez, D., Oughton, S., and Montgomery, D., 1991, "Selective Decay and Coherent Vortices in Two-Dimensional Incompressible Turbulence," Phys. Rev. Lett., **66**, pp. 2731–2734.
[85] Montgomery, D., Matthaeus, W. H., Stribling, W. T., Martinez, D., and Oughton, S., 1992, "Relaxation in Two Dimensions and the 'Sinh-Poisson' Equation," Phys. Fluids A, **4**, pp. 3–6.
[86] Joyce, G. R., and Montgomery, D., 1973, "Negative Temperature States for the Two-Dimensional Guiding Centre Plasma," J. Plasma Phys., **10**, pp. 107–121.
[87] Montgomery, D., and Joyce, G. R., 1974, "Statistical Mechanics of Negative Temperature States," Phys. Fluids, **17**, pp. 1139–1145.
[88] Pointin, Y. B., and Lundgren, T. S., 1976, "Statistical Mechanics of Two-Dimensional Vortices in a Bounded Domain," Phys. Fluids, **19**, pp. 1459–1470.
[89] Ting, A. C., Chen, H. H., and Lee, Y. C., 1987, "Exact Solution of a Nonlinear Boundary Value Problem: The Vortices of the Two-Dimensional Sinh-Poisson Equation," Physica D, **26**, pp. 37–66.
[90] Miller, J., 1990, "Statistical Mechanics of Euler's Equation in Two Dimensions," Phys. Rev. Lett., **65**, pp. 2137–2140.
[91] Miller, J., Weichman, P. B., and Cross, M. C., 1992, "Statistical Mechanics, Euler's Equation, and Jupiter's Red Spot," Phys. Rev. A, **45**, pp. 2328–2359.
[92] Robert, R., and Sommeria, J., 1991, "Statistical Equilibrium States for Two-Dimensional Flow," J. Fluid Mech., **229**, pp. 291–310.
[93] Chavanis, P. H., and Sommeria, J., 1996, "Classification of Self-Organized Structures in Two-Dimensional Turbulence: The Case of a Bounded Domain," J. Fluid Mech., **314**, pp. 267–297.
[94] Danilov, S., Dolzhanskii, F. V., Dovzhenko, V. A., and Krymov, V. A., 2002, "Experiments on Free Decay of Quasi-Two-Dimensional Turbulent Flows," Phys. Rev. E, **65**, p. 036316.
[95] Clercx, H. J. H., van Heijst, G. J. F., and Zoeteweij, M. L., 2003, "Quasi-Two-Dimensional Turbulence in Shallow Fluid Layers: The Role of Bottom Friction and Fluid Layer Depth," Phys. Rev. E, **67**, p. 066303.
[96] Wells, J., and Afanasyev, Ya. D., 2004, "Decaying Quasi-Two-Dimensional Turbulence in a Rectangular Container: Laboratory Experiments," Geophys. Astrophys. Fluid Dyn., **98**, pp. 1–20.
[97] Rivera, M. K., and Ecke, R. E., 2005, "Pair Dispersion and Doubling Time Statistics in Two-Dimensional Turbulence," Phys. Rev. Lett., **95**, p. 194503.
[98] Boffetta, G., Cenedese, A., Espa, S., and Musacchio, S., 2005, "Effects of Friction on 2D Turbulence: An Experimental Study of the Direct Cascade," Europhys. Lett., **71**, pp. 590–596.
[99] Shats, M. G., Xia, H., and Punzmann, H., 2005, "Spectral Condensation of Turbulence in Plasma and Fluids and Its Role in Low-to-High Phase Transitions in Toroidal Plasmas," Phys. Rev. E, **71**, p. 046409.
[100] Akkermans, R. A. D., Kamp, L. P. J., Clercx, H. J. H., and van Heijst, G. J. F., 2008, "Intrinsic Three-Dimensionality in Electromagnetically Driven Shallow Flows," EPL, **83**, p. 24001.
[101] Akkermans, R. A. D., Cieslik, A. R., Kamp, L. P. J., Trieling, R. R., Clercx, H. J. H., and van Heijst, G. J. F., 2008, "The Three-Dimensional Structure of an Electromagnetically Generated Dipolar Vortex in a Shallow Fluid Layer," Phys. Fluids, **20**, p. 116601.
[102] Sommeria, J., 1986, "Experimental Study of the Two-Dimensional Inverse Energy Cascade in a Square Box," J. Fluid Mech., **170**, pp. 139–168.
[103] We adopt for this and other experiments a Cartesian coordinate frame, with the x- and y-axis spanning a plane parallel to the bottom of the tank, and the z-axis is taken vertically upward.
[104] Verron, J., and Sommeria, J., 1987, "Numerical Simulation of a Two-Dimensional Turbulence Experiment in Magnetohydrodynamics," Phys. Fluids, **30**, pp. 732–739.
[105] Molenaar, D., Clercx, H. J. H., and van Heijst, G. J. F., 2004, "Angular Momentum of Forced 2D Turbulence in a Square No-Slip Domain," Physica D, **196**, pp. 329–340.
[106] Tabeling, P., Burkhart, S., Cardoso, O., and Willaime, H., 1991, "Experimental Study of Freely Decaying Two-Dimensional Turbulence," Phys. Rev. Lett., **67**, pp. 3772–3775.
[107] Dolzhanskii, F. V., Krymov, V. A., and Manin, D. Yu., 1992, "An Advanced Experimental Investigation of Quasi-Two-Dimensional Shear Flows," J. Fluid Mech., **241**, pp. 705–722.
[108] Jüttner, B., Marteau, D., Tabeling, P., and Thess, A., 1997, "Numerical Simulations of Experiments on Quasi-Two-Dimensional Turbulence," Phys. Rev. E, **55**, pp. 5479–5488.
[109] Marteau, D., Cardoso, O., and Tabeling, P., 1995, "Equilibrium States of Two-Dimensional Turbulence: An Experimental Study," Phys. Rev. E, **51**, pp. 5124–5127.
[110] Paret, J., Marteau, D., Paireau, O., and Tabeling, P., 1997, "Are Flows Electromagnetically Forced in Thin Stratified Layers Two-Dimensional?" Phys. Fluids, **9**, pp. 3102–3104.
[111] Clercx, H. J. H., Maassen, S. R., and van Heijst, G. J. F., 1999, "Decaying Two-Dimensional Turbulence in Square Containers With No-Slip or Stress-Free Boundaries," Phys. Fluids, **11**, pp. 611–626.
[112] Satijn, M. P., Cense, A. W., Verzicco, R., Clercx, H. J. H., and van Heijst, G. J. F., 2001, "Three-Dimensional Structure and Decay Properties of Vortices in Shallow Fluid Layers," Phys. Fluids, **13**, pp. 1932–1945.
[113] Note that $\lim_{\lambda\to 0} t_* = t$ and $t_* \approx t$ if $t \lesssim \mathrm{Re}_\lambda$.
[114] It is found more appropriate to use the typical eddy turnover time of the initial vortices in the discussion of the numerical results. For the simulations discussed in this section, $\tau \approx 4t$.
[115] Paret, J., and Tabeling, P., 1997, "Experimental Observation of the Two-Dimensional Inverse Energy Cascade," Phys. Rev. Lett., **79**, pp. 4162–4165.
[116] Paret, J., and Tabeling, P., 1998, "Intermittency in the Two-Dimensional Inverse Cascade of Energy: Experimental Observations," Phys. Fluids, **10**, pp. 3126–3136.
[117] The notation, although commonly used, might be somewhat confusing. Strictly spoken it is the statistical average that depends solely on $r=|\mathbf{r}|$ and not on $\mathbf{x}$; thus $\langle|\delta u_{\|}(\mathbf{x},\mathbf{r})|^n\rangle = f(r)$.
[118] Dubos, T., Babiano, A., Paret, J., and Tabeling, P., 2001, "Intermittency and Coherent Structures in the Two-Dimensional Inverse Energy Cascade: Comparing Numerical and Laboratory Experiments," Phys. Rev. E, **64**, p. 036302.
[119] Paret, J., Jullien, M.-C., and Tabeling, P., 1999, "Vorticity Statistics in the Two-Dimensional Enstrophy Cascade," Phys. Rev. Lett., **83**, pp. 3418–3421.
[120] Falkovich, G., and Lebedev, V., 1994, "Universal Direct Cascade in Two-Dimensional Turbulence," Phys. Rev. E, **50**, pp. 3883–3899.
[121] Eyink, G. L., 1995, "Exact Results on Scaling Exponents in the 2D Enstrophy Cascade," Phys. Rev. Lett., **74**, pp. 3800–3803.
[122] Nam, K., Ott, E., Antonsen, T. M., Jr., and Guzdar, P. N., 2000, "Lagrangian Chaos and the Effect of Drag on the Enstrophy Cascade in Two-Dimensional Turbulence," Phys. Rev. Lett., **84**, pp. 5134–5137.
[123] Boffetta, G., Celani, A., Musacchio, S., and Vergassola, M., 2002, "Intermittency in Two-Dimensional Ekman-Navier-Stokes Turbulence," Phys. Rev. E, **66**, p. 026304.
[124] Wells, M. G., Clercx, H. J. H., and van Heijst, G. J. F., 2007, "Vortices in Oscillating Spin-Up," J. Fluid Mech., **573**, pp. 339–369.
[125] van Heijst, G. J. F., Clercx, H. J. H., and Molenaar, D., 2006, "The Effects of Solid Boundaries on Confined Two-Dimensional Turbulence," J. Fluid Mech., **554**, pp. 411–431.
[126] Maassen, S. R., Clercx, H. J. H., and van Heijst, G. J. F., 2002, "Self-

Organization of Quasi-2D Turbulence in Stratified Fluids in Square and Circular Containers," Phys. Fluids, **14**, pp. 2150–2169.
[127] Clercx, H. J. H., Maassen, S. R., and van Heijst, G. J. F., 1998, "Spontaneous Spin-Up During the Decay of 2D Turbulence in a Square Container With Rigid Boundaries," Phys. Rev. Lett., **80**, pp. 5129–5132.
[128] Maassen, S. R., Clercx, H. J. H., and van Heijst, G. J. F., 2003, "Self-Organization of Decaying Quasi-2D Turbulence in Stratified Fluids in Rectangular Containers," J. Fluid Mech., **495**, pp. 19–33.
[129] Li, S., and Montgomery, D., 1996, "Decaying Two-Dimensional Turbulence With Rigid Walls," Phys. Lett. A, **218**, pp. 281–291.
[130] Li, S., Montgomery, D., and Jones, W. B., 1996, "Inverse Cascades of Angular Momentum," J. Plasma Phys., **56**, pp. 615–639.
[131] Li, S., Montgomery, D., and Jones, W. B., 1997, "Two-Dimensional Turbulence With Rigid Circular Walls," Theor. Comput. Fluid Dyn., **9**, pp. 167–181.
[132] Equivalence of both terms can also be shown by expressing the pressure boundary condition for the present problem in terms of the normal vorticity gradient at the no-slip boundary.
[133] Clercx, H. J. H., 1997, "A Spectral Solver for the Navier-Stokes Equations in the Velocity-Vorticity Formulation for Flows With Two Non-Periodic Directions," J. Comput. Phys., **137**, pp. 186–211.
[134] Daube, O., 1992, "Resolution of the 2D Navier-Stokes Equations in Velocity-Vorticity Form by Means of an Influence Matrix Technique," J. Comput. Phys., **103**, pp. 402–414.
[135] Clercx, H. J. H., and Bruneau, C.-H., 2006, "The Normal and Oblique Collision of a Dipole With a No-Slip Boundary," Comput. Fluids, **35**, pp. 245–279.
[136] Orszag, S. A., 1969, "Numerical Methods for the Simulation of Turbulence," Phys. Fluids, **12**, pp. II-250–II-257.
[137] Kress, B. T., and Montgomery, D. C., 2000, "Pressure Determinations for Incompressible Fluids and Magnetofluids," J. Plasma Phys., **64**, pp. 371–377.
[138] Maassen, S. R., Clercx, H. J. H., and van Heijst, G. J. F., 1999, "Decaying Quasi-2D Turbulence in a Stratified Fluid With Circular Boundaries," Europhys. Lett., **46**, pp. 339–345.
[139] Yap, C. T., and van Atta, C. W., 1993, "Experimental Studies of the Development of Quasi-Two-Dimensional Turbulence in Stably Stratified Fluid," Dyn. Atmos. Oceans, **19**, pp. 289–323.
[140] Fincham, A. M., Maxworthy, T., and Spedding, G. R., 1996, "Energy Dissipation and Vortex Structure in Freely Decaying Stratified Grid Turbulence," Dyn. Atmos. Oceans, **23**, pp. 155–169.
[141] Schneider, K., and Farge, M., 2005, "Decaying Two-Dimensional Turbulence in a Circular Container," Phys. Rev. Lett., **95**, p. 244502.
[142] Clercx, H. J. H., and van Heijst, G. J. F., 2002, "Dissipation of Kinetic Energy in Two-Dimensional Bounded Flows," Phys. Rev. E, **65**, p. 066305.
[143] Clercx, H. J. H., and van Heijst, G. J. F., 2000, "Energy Spectra for Decaying 2D Turbulence in a Bounded Domain," Phys. Rev. Lett., **85**, pp. 306–309.
[144] Angot, P., Bruneau, C.-H., and Fabrie, P., 1999, "A Penalization Method to Take Into Account Obstacles in Viscous Flows," Numer. Math., **81**, pp. 497–520.
[145] Arquis, E., and Caltagirone, J. P., 1984, "Sur les conditions hydrodynamique au voisinage d'une interface milieu fluide-milieu poreux: Application à la convection naturelle," C. R. Acad. Sci., Ser. II: Mec., Phys., Chim., Sci. Terre Univers, **299**, pp. 1–4.
[146] Keetels, G. H., D'Ortona, U., Kramer, W., Clercx, H. J. H., Schneider, K., and van Heijst, G. J. F., 2007, "Fourier Spectral and Wavelet Solvers for the Incompressible Navier–Stokes Equations With Volume-Penalization: Convergence of a Dipole-Wall Collision," J. Comput. Phys., **227**, pp. 919–945.
[147] Keetels, G. H., Clercx, H. J. H., and van Heijst, G. J. F., 2009, "The Origin of Spin-Up Processes in Decaying Two-Dimensional Turbulence," Eur. J. Mech. B/Fluids, submitted.

Herman J. H. Clercx *is Professor in Transport in Turbulent Flows at Eindhoven University of Technology (the Netherlands) and holds a part-time chair in Mathematical Modelling of Geophysical Flows at Twente University, the Netherlands. He received his MSc degree in (theoretical) physics in 1987 from Radboud University Nijmegen (the Netherlands) and subsequently his Ph.D. degree in physics in 1991 from Eindhoven University of Technology. After a stay of one year as post doctoral fellow at the University of Nice (France), where he worked on electro- and magneto-rheological fluids, he returned in 1993 to Eindhoven University of Technology. His research interests include (quasi-)2D turbulence, turbulence affected by stratification and/or rotation, (inertial) particle dispersion and particle collisions in turbulence, multiscale modelling of transport in turbulent flows, pseudospectral methods for turbulence simulations, and 3D viscous mixing problems for microfluidic and industrial applications.*

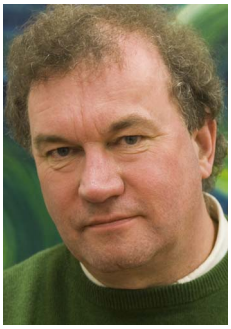

GertJan van Heijst *is a Professor of Fluid Dynamics in the Department of Physics at Eindhoven University of Technology, The Netherlands. He received his Ph.D. degree from the Twente University (NL) in 1981. After a postdoctoral position at the University of Cambridge (UK), he became a lecturer (Associate Professor) at the Institute of Meterorology and Oceanography at the University of Utrecht (NL). In 1990 he got a full chair in Eindhoven. His research interests include vortices and turbulence in rotating and stratified flows, two-dimensional turbulence, and viscous mixing. Until recently he was Associate Editor of Physics of Fluids and of Geophysical and Astrophysical Fluid Dynamics, and he is co-editor-in-chief of the European Journal of Mechanics B/Fluids. He is one of the local directors of the J M Burgers Centre and member of the Royal Netherlands Academy of Arts and Sciences.*